2015-06-18

Numerical Modeling of Onshore Plankton Transport

Atsushi Fujimura
University of Miami, afujimura@rsmas.miami.edu

UNIVERSITY OF MIAMI

NUMERICAL MODELING OF ONSHORE PLANKTON TRANSPORT

By

Atsushi Fujimura

A DISSERTATION

Submitted to the Faculty
of the University of Miami
in partial fulfillment of the requirements for
the degree of Doctor of Philosophy

Coral Gables, Florida

August 2015

UNIVERSITY OF MIAMI

A dissertation submitted in partial fulfillment of
the requirements for the degree of
Doctor of Philosophy

NUMERICAL MODELING OF ONSHORE PLANKTON TRANSPORT

Atsushi Fujimura

Approved:

_____
Ad Reniers, Ph.D.
Professor of Hydraulic Engineering
Delft University of Technology

_____
Claire Paris, Ph.D.
Associate Professor of
Applied Marine Physics

_____
Josefina Olascoaga, Ph.D.
Associate Professor of
Applied Marine Physics

_____
Alan Shanks, Ph.D.
Professor of Biology
University of Oregon

_____
Steven Morgan, Ph.D.
Professor of Biology
University of California, Davis

_____
Dean of the Graduate School

_____
Jamie MacMahan, Ph.D.
Associate Professor of Oceanography
Naval Postgraduate School
Monterey, California

FUJIMURA, ATSUSHI (Ph.D., Applied Marine Physics)
Numerical Modeling of Onshore Plankton Transport. (August 2015)

Abstract of a dissertation at the University of Miami.

Dissertation supervised by Professors Ad Reniers and Claire Paris.
No. of pages in text. (70)

Cross-shore exchange of plankton plays an important role in marine ecosystems and coastal communities. Larvae of many intertidal invertebrate species grow offshore and come back to the shore for settlement by crossing the energetic surf zone: however, shoreward transport mechanisms are not well understood. To test the possible onshore transport mechanisms, numerical simulations are performed based on the field campaigns conducted at Sand City beach (a mildly sloping rip-channeled beach) and Carmel River State Beach (CRSB, a steep pocket beach). The model consists of the 3D hydrodynamic model Delft3D and an individual based model for larval tracking. As weak swimmers, many invertebrate larvae are greatly controlled by currents, but biological factors such as larval buoyancy and turbulent-dependent sinking behavior also play important roles. Depending on the vertical positions of larvae, wave-induced bottom boundary layer streaming or wind-driven surface currents carry larvae toward the shore. Stokes drift is necessary to achieve onshore larval migration for all cases. In addition, beach morphology and coastal configurations affect larval distribution patterns and their concentrations. Model results show that onshore larval delivery rate is higher at a mild sloping beach than at a reflective beach, consistent with literature and the field observations along the California coast. Furthermore, alongshore variability is also

important for larval migration toward the shore. Rip channels induce rip currents as well as feeder currents (i.e., shoaling), and enhance cross-shore exchange. Wave group also acts as additional forcing to the cross-shore material exchange by producing transient rip currents. This model study confirms that all physical, biological, and geological regimes determine onshore larval transport patterns.

Acknowledgements

I am grateful to my advisors Ad Reniers and Claire Paris, and my dissertation committee members Alan Shanks, Jamie MacMahan, Steven Morgan, and Josefina Olascoaga for assistance in my research and dissertation. I also appreciate my colleagues, technicians, and students who helped with the field experiments. This study is supported by National Science Foundation (NSF) Ocean Sciences (OCE-092735) 'Collaborative Research: Does coupling between the inner shelf and surf zone regulate larval supply to intertidal populations?'. This project is a contribution of the Rosenstiel School of Marine and Atmospheric Science, the Oregon Institute of Marine Biology, the Naval Postgraduate School, and the Bodega Marine Laboratory. Last but not least, I thank my family, friends, and the RSMAS community for their support and encouragement.

TABLE OF CONTENTS

Page

LIST OF FIGURES

LIST OF TABLES

Chapter 1

INTRODUCTION

1.1. Background

Larval recruitment is an important element in the dynamics and structure of marine populations and communities. Larvae of many intertidal invertebrates cross the surf zone, develop in the open ocean, and migrate back to the shore at the end of the larval stage (Morgan et al. 2009c, Shanks & Shearman 2009). Most invertebrate larvae are slow swimmers (Mileikovsky 1973, Chia et al. 1984) that regulate depth and likely depend on currents and other physical forcing to transport them onshore for settlement (Queiroga & Blanton 2005). In upwelling regimes along the western margins of continents, a widely accepted hypothesis is that larvae of intertidal invertebrates are swept offshore during wind-driven upwelling events (Roughgarden et al. 1988, Connolly et al. 2001). However, recent studies conducted in northern California (Morgan et al. 2009a, b, c, Morgan & Fisher 2010) and southern Oregon (Shanks & Shearman 2009) revealed that the onshore transport of larvae of many invertebrates is not limited by upwelling. Additionally, larvae of most species were not carried far offshore by upwelling nor onshore by downwelling, but were found at all times within several kilometers of shore; competent larvae (ready to settle) were abundant within a kilometer from shore during the summer (Shanks & Shearman 2009, Morgan & Fisher 2010). More importantly, onshore recruitment of these competent larvae was spatially and temporally variable, suggesting the hypothesis that the surf zone may represent a semi-permeable barrier to cross-shore exchange (Rilov et al. 2008, Shanks et al. 2010). Local processes

within the surf zone are important for the migration of the larvae of intertidal invertebrate; however, the mechanism of larval delivery across this barrier is not understood.

There are a number of possible physical transport mechanisms that need to be considered. At a heterogeneous shore with alongshore-sandbars, shoals and rip channels produce rip currents, which can enhance cross-shore exchange (Talbot & Bate 1987, Clarke et al. 2007, MacMahan et al. 2010, Reniers et al. 2009, 2010). Onshore transport mainly occurs over shoals where wave breaking occurs driving onshore flows that diverge towards the shore and subsequently feed strong offshore-directed rip currents. Rip-channeled beaches are common and observed around the world. This rip-channeled system of alongshore variability-induced exchange is generally found at intermediate (gradual beach slope) beaches and not at reflective (steep beach slope) beaches (Wright & Short 1984), which is consistent with observations by Shanks et al. (2010) who showed that recruitment was higher on mildly sloping beaches than on steep beaches.

Stokes drift (Stokes 1847) is a time-averaged volume transport current in the direction of wave propagation, and it may slowly transport larvae toward shore. This mechanism may be active at dissipative beaches, but might not or only partially be supported at reflective beaches as Stokes drift is associated with progressive surface gravity waves only, and steep beaches reflect waves with a wide range of frequencies resulting in (partially) standing waves. Stokes drift is explained further in the Methods section.

Cross-shore wind forcing also can increase cross-shore exchange (Tilburg 2003, Fewings et al. 2008). Surface mass transport is in the direction of wind forcing, so

onshore wind may push larvae near the surface toward shore. For offshore wind or weak wind conditions, surface currents flow in the opposite direction (Lentz et al. 2008).

Wave stress in the bottom boundary layer generates persistent streaming in the direction of wave propagation (Longuet-Higgins 1953). Although streaming velocities are small (O, cm s^{-1}), over time, they may cause onshore transport of larvae near the bottom.

Most invertebrate larvae are slow swimmers (Mileikovsky 1973, Chia et al. 1984) that depend largely on water currents and other physical forcing during their onshore migration; however, at spatial scales smaller than $O(10)$ m, biotic processes should not be ignored (Butman 1987). Thus, in addition to the physical forcing, biological factors such as buoyancy, sinking rate and depth preferences of larvae may also need to be taken into account. By regulating their depth, larvae of some species recruit onshore in surface waters, whereas other species recruit onshore near the bottom in upwelling regimes (Morgan et al. 2009a). Larvae of some intertidal invertebrate species are known to behave as passive particles and sink to the bottom in turbulence such as the surf zone (Butman 1989, Denny & Shibata 1989, Fuchs et al. 2004, Roy et al. 2013). Oyster larvae (*Crassostrea virginica*) can even actively move downward in turbulence (Fuchs et al. 2013). These behaviors could enhance their settlement success.

Tracking larvae in a very turbulent and rough environment is not feasible. However, biophysical numerical modeling allows examining the discrete and combined roles of physical and biological processes in the surf zone. Particularly, an Individual Based Model (IBM) with complex hydrodynamics is quite useful for modeling microscopic organisms in various flow conditions and has been extensively used in

population connectivity studies (Paris et al. 2007). Possible mechanisms of onshore larval delivery are tested by using a similar technique based on a newly established coupled modeling system (Paris et al. 2013).

1.2. Objectives and Overview

The main purpose of this project is to determine how competent larvae cross the surf zone at the last stage of their migration.

In Chapter 2, possible mechanisms of onshore larval transport at a rip-channeled beach are identified. Preliminary model result showed that passive particles are mostly flushed offshore, so some parameters other than wave-induced currents need to be included. The effects of Stokes drift, wind forcing, and vertical motions of larvae (i.e., buoyancy and sinking behavior) are tested. I also study the effects of random wave groups that could generate more realistic situations, such as infragravity waves and surf zone eddies, than regular waves (MacMahan et al. 2004, Reniers et al. 2010). Model results are compared to data from field study showing that larvae are highly concentrated in rip-channels. In addition to finding possible mechanisms of onshore larval migration at a rip-channeled beach, Chapter 2 also contributes to establish a biophysical modeling method used throughout the dissertation.

In Chapter 3, onshore larval transport is modeled on a steep pocket beach. Transport pattern on this beach is different from the rip-channeled beach. In fact, preliminary field data and model results revealed a strong alongshore current that affects larval transport. Field data also show a correlation between concentration of competent larvae and detritus in the surf zone, so transport of detritus is also simulated.

Additionally, it is predicted that larval concentration in the surf zone is inversely correlated with wave height as the field data shown.

Beach morphology largely affect larval transport as shown in Chapters 2 and 3; however, it is difficult to identify how each morphological characteristic of beach influence onshore larval transport rates. In Chapter 4, the beach characteristics are decomposed into simple forms. Modeling with alongshore uniform beaches show that a mild sloping beach attracts more larvae than a steeper beach. Larvae also get into the surf zone easier at a rip-channeled beach because of the shoaling effect than at an alongshore uniform beach. In addition to steady wave forcing, wave group is also tested to see if it adds an extra forcing on cross-shore exchange.

A dissertation summary and conclusions are presented in Chapter 5. Future work and directions are also given.

Chapter 2

LARVAL TRANSPORT INTO A RIP-CHANNELED BEACH

2.1. Introductory Remarks

In this chapter, onshore larval transport in various physical regimes (Stokes drift, wind stress, and wave group forcing) with biological parameters (buoyancy and sinking behavior of larvae) are examined at moderate sloping rip-channeled beach to provide possible mechanisms of onshore larval migration. Model results are compared to the data from the field survey. The basics of biophysical model established in this chapter are also applied to simulations in the other chapters.

2.2. Field Survey

Physical data and biological samples were collected at Sand City beach, Monterey Bay, California in the summer of 2010 (Fig. 2.1A). The location is characterized as an intermediate beach (moderate beach slope, Wright & Short 1984) with well-formed rip channels and shoals. Bathymetric data used for the model grid were collected with a personal watercraft equipped with sonar and a Global Positioning System (GPS), and for the near shore, a person walking with a GPS. The alongshore-average beach profile consists of 1/7.5 intertidal beach slope, 1/57 surf zone slope, and 1/25 offshore profile. Alongshore variability in the beach profile is apparent in Fig. 2.1B. Current and wave data were obtained by acoustic Doppler current profilers located at 11 m water depth.

Replicate plankton samples were collected repeatedly for 30 days (15 June to 15 July 2010) at three locations: offshore just outside the surf zone (inner shelf), rip channel, and shoal (Fig. 2.1B). Within the rip channel and on the shoal a zooplankton net with 202

μm mesh and a 25 cm diameter equipped with a flow meter was used to collect the samples as the horizontal flow pushed through the net. Just outside of the surf zone, an identical net was used to collect the zooplankton samples by hauling the net from the bottom to the surface. A summary graph of zooplankton concentrations at the three locations is shown in the discussion section to compare with the model output.

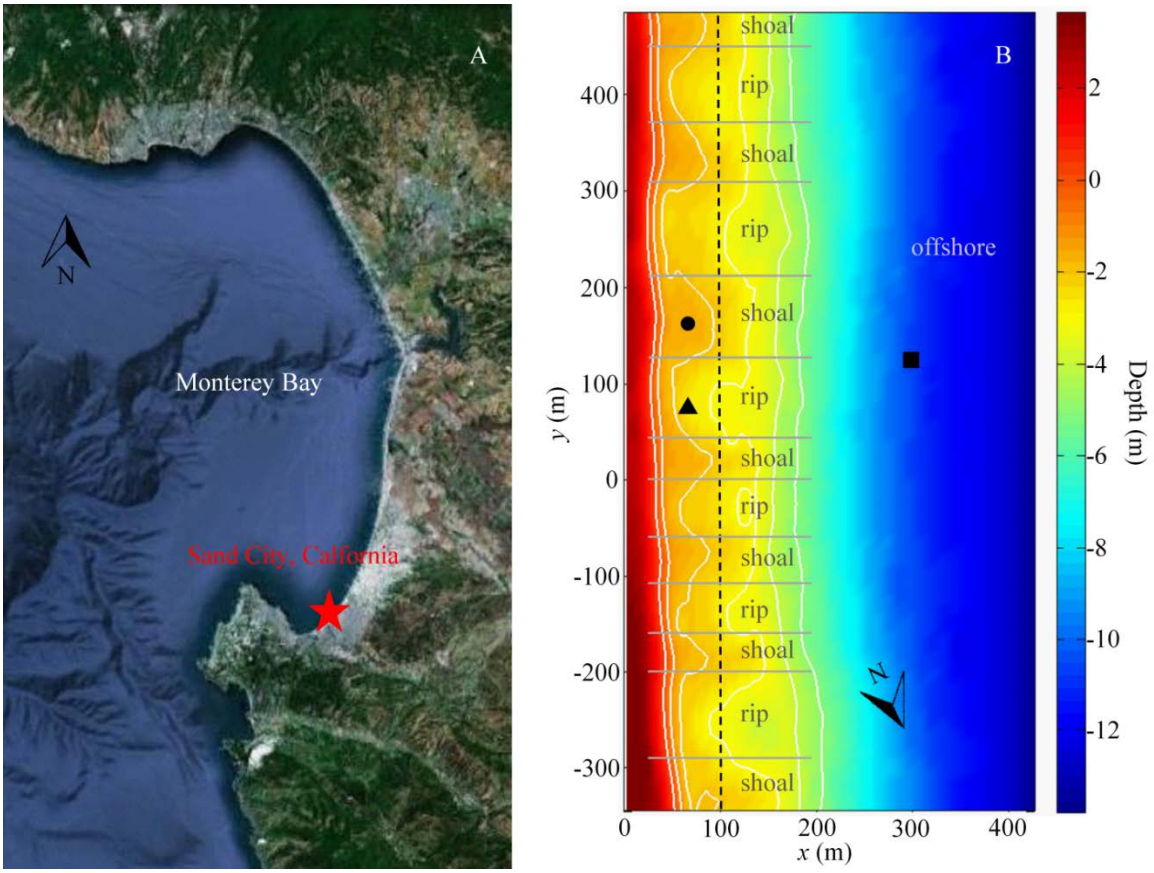

Fig. 2.1. (A) The study site is indicated by a red star (credit: Google Earth). (B) Bathymetry in the model domain. White isobaths are in 1 m increments from 0 m (shoreline) to 5 m. The approximate edge of the surf zone is shown as a black dashed line. North is to the bottom. Rip channel and shoal ranges are shown. The approximate plankton sampling locations are indicated in a circle for the shoal, a triangle for the rip channel, and a square for offshore.

2.3. Numerical Simulations

2.3.1. Hydrodynamic model

The numerical simulation software package Delft3D is used to perform three-dimensional hydrodynamic model simulations of the nearshore. The Delft3D hydrodynamic model comprises FLOW (Deltares 2013a) and WAVE (Deltares 2013b) modules.

The model domain forms of 850 m in the alongshore direction, 450 m in cross-shore direction, and collected bathymetry data determined depths. A regular grid (hexahedral cells) is used for the model mesh. Spacing of grid cells is 10 m alongshore, approximately 5–10 m cross-shore with the finest resolution at the shoreline, and 14 σ-layers are applied for vertical spacing, which become finer toward the bottom to resolve boundary layer streaming. Shoreline reflections are managed by an offshore Riemann boundary, a weakly reflective open boundary, while the other sides (onshore and alongshore) are closed. Turbulence is modeled with a k-ε closure scheme (Deltares 2013a), with transport equations to solve turbulent kinetic energy (k) and energy dissipation rate (ε).

Shore normal waves, based on the average wave data during the biological sampling period (significant wave height = 0.75 m, peak wave period = 8.75 s), are generated at the offshore boundary. Two wave conditions are applied: regular normally incident waves and random wave groups by using the Joint North Sea Wave Project (JONSWAP) spectrum (Hasselmann et al. 1973). I also test effects of wind surface stress by applying either no wind (0 m s^{-1}) or constant onshore wind (8.0 m s^{-1}), which represent minimal and peak wind speeds measured during the field experiment, respectively.

Run time is 2 h with a time step of 3 s, and intervals of output and communication between FLOW and WAVE are 6 s. Because no diurnal events (tide, various wind, etc.) are considered, the 2 h simulation output is used periodically for a 24 h larval transport simulation. The model domain and bathymetry are shown in Fig. 2.1B.

2.3.2. Larval transport model

Modeled physical parameters, such as currents, waves, bathymetry, eddy diffusivities and turbulence, are transferred to a biological module. This module is adapted from the Connectivity Modeling System (CMS, Paris et al. 2013*b*), which is a coupled multi-scale biophysical IBM, based on a stochastic Lagrangian framework. The CMS code is rewritten in a MATLAB with some modifications to directly import the physical model output. The imported outputs include the bathymetry, water levels, flow velocities, wave information, eddy diffusivities, and turbulent energy dissipation rate every 6 s.

A 4th order Runge-Kutta method is used for integration of the advection part, both in time and space following Paris et al. (2013*b*):

$$k_1 = f\left(\vec{U}_i, t_i\right)\Delta t \qquad (1)$$

$$k_2 = f\left(\vec{U}_i + \frac{k_1}{2}, t_i + \frac{\Delta t}{2}\right)\Delta t \qquad (2)$$

$$k_3 = f\left(\vec{U}_i + \frac{k_2}{2}, t_i + \frac{\Delta t}{2}\right)\Delta t \qquad (3)$$

$$k_4 = f\left(\vec{U}_i + k_3, t_i + \Delta t\right)\Delta t \qquad (4)$$

$$\vec{U}_{i+1} = \vec{U}_i + \frac{k_1 + 2k_2 + 2k_3 + k_4}{6} \qquad (5)$$

where $\vec{U}$ is the velocity of water current at *i*th time step. The integration time step size Δt is 6 s, where the spatial resolution is the same as the one used in the physical model.

The velocity $\vec{U}$ in Eqs.1-5 is set as either Eulerian (background) velocity or Lagrangian (particle tracking) velocity to test the effect of Stokes drift. Their relationship is,

$$\vec{U}_L = \vec{U}_E + \vec{U}_S \qquad (6)$$

where $\vec{U}_L$ is the Lagrangian velocity, $\vec{U}_E$ is the Eulerian velocity, and $\vec{U}_S$ is Stokes drift written as,

$$\vec{U}_S = \frac{\omega k a^2 \cosh(2k(H+z))}{2\sinh^2(kH)}(\cos\phi, \sin\phi) \qquad (7)$$

where ω is the radial wave frequency, k is the radial wave number, a is the wave amplitude, H is the local water depth, z is the vertical position of a particle with $z = 0$ at mean sea level, and ϕ is the wave angle. In this study, I neglect potential entrainment of particles in the breaking wave roller (Feddersen 2007, Reniers et al. 2013), which may contribute to the preferential transport of surface material from the shoals to the rip channels that experience less wave breaking due to their increased depth, but at present cannot be resolved within this three-dimensional modeling approach.

I apply a random walk to each particle to account for subgrid-scale turbulence. This is modeled by adding random velocities u_{diff}, v_{diff}, w_{diff} of all three spatial components (cross-shore, alongshore, and vertical direction, respectively) calculated by,

$$u_{\text{diff}} = n\sqrt{\frac{2K_h}{\Delta t}} \qquad (8)$$

$$v_{\text{diff}} = n\sqrt{\frac{2K_h}{\Delta t}} \qquad (9)$$

$$w_{\text{diff}} = n\sqrt{\frac{2K_v}{\Delta t}} \qquad (10)$$

where n is a Gaussian random number, K_h and K_v are horizontal and vertical eddy diffusivities, respectively.

Each particle is assigned a vertical velocity w_b, which represents buoyancy or vertical swimming speed of the larva. I test three types of w_b: 0 m s^{-1} (neutrally buoyant), -10^{-3} m s^{-1} (negatively buoyant) and 4×10^{-3} m s^{-1} (positively buoyant) based on Fuchs et al. (2004). No active horizontal swimming behavior is considered here.

I also test a scenario that a larva stops swimming vertically and sinks by its own weight in the presence of turbulence. According to Fuchs et al. (2004), competent larvae sink at $w_s = -10^{-2}$ m s^{-1} when the turbulent energy dissipation rate is $\varepsilon > 10^{-5}$ m^2 s^{-3}. In this dissertation, this type of behavior is called sinking behavior.

Thus, the total velocity components u_{tot} (cross-shore), v_{tot} (alongshore), and w_{tot} (vertical) are,

$$u_{\text{tot}} = u_{\text{adv}} + u_{\text{diff}} \qquad (11)$$

$$v_{\text{tot}} = v_{\text{adv}} + v_{\text{diff}} \qquad (12)$$

$$w_{\text{tot}} = \begin{cases} w_{\text{adv}} + w_{\text{diff}} + w_b & \text{if the sinking behavior is off} \\ w_{\text{adv}} + w_{\text{diff}} + w_b & \varepsilon < 10^{-5}\,\text{m}^2\text{s}^{-3} \\ w_{\text{adv}} + w_{\text{diff}} + w_s & \varepsilon \geq 10^{-5}\,\text{m}^2\text{s}^{-3} \end{cases} \qquad (13)$$

where u_{adv}, v_{adv}, and w_{adv} are advection flow velocities of the three spatial components from Eq. 5. And then, a new position of the particle is,

$$\vec{X}_{i+1} = \vec{X}_i + \vec{U}_{\text{tot}}\Delta t \qquad (14)$$

where $\vec{X}_i$ is the old position of all three spatial components and $\vec{U}_{\text{tot}}$ is the total velocity obtained from Eqs. 11-13.

During a 24 h simulation, 602 particles (86 × 7 array) are released every hour from offshore (x = 410 m) equally distributed alongshore (Δy = 10 m) at three vertical locations for each type of particle: near the bottom for the particles with negative buoyancy, near the water surface for the ones with positive buoyancy, and dispersed through water column for the ones with neutral buoyancy (Fig. 2.2). The number of particles and the release frequency are due to limited computational ability, but sufficient for the main purpose since the sensitivity analysis, as recommended by North et al. (2009), showed that the main results do not change with at least half the number of particles. Offshore and alongshore boundaries are set as outlets, so once a particle crossed one of the boundaries, it is no longer taken into account. The first 12 h run is used as a spin-up stage for particle initialization. The second half of the simulation (12-24 h) is used to calculate the time-averaged number of particles. The test cases and model parameters are summarized in Table 2.1.

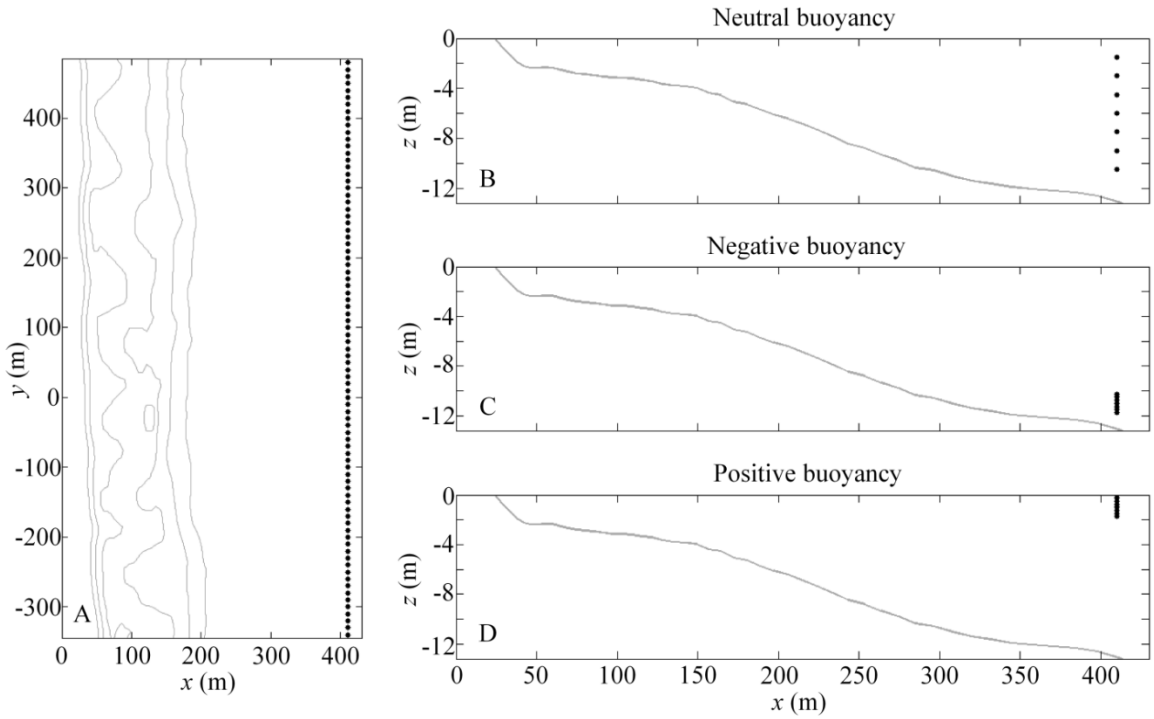

Fig. 2.2. Initial location of particles shown in black dots. (A) Horizontal distribution for all types of particles. Bottom contour lines from 0 m depth (shore line) to 5 m depth with 1 m increments are given. Vertical distributions of (B) neutrally buoyant, (C) negatively buoyant, and (D) positively buoyant particles. The maximum depth line is shown in gray.

Table 2.1. Performed model cases. In the 'Wave' column, 'regular' is regular incident wave, and 'group' is random wave group. 'Wind' is either no wind (0 m s^{-1}) or onshore wind (8.0 m s^{-1}). w_s = sinking behavior of particles, included (on) or not (off). w_b = vertical velocity of particles. $\vec{U}_S$ = Stokes drift, either included (on) or not (off). Each case name describes a test condition: 's' if sinking behavior is included; 'w' if onshore wind is included; '0', '-', or '+' correspond to neutral, negative, or positive buoyancy of particles, respectively.

Case	Wave	Wind (m s^{-1})	w_s	w_b (m s^{-1})	$\vec{U}_S$
1.0	regular	0	off	0	on
2.-	regular	0	off	-10^{-3}	on
3.+	regular	0	off	4×10^{-3}	on
4.s0	regular	0	on	0	on
5.s-	regular	0	on	-10^{-3}	on
6.s+	regular	0	on	4×10^{-3}	on
7.w0	regular	8.0	off	0	on
8.w-	regular	8.0	off	-10^{-3}	on
9.w+	regular	8.0	off	4×10^{-3}	on
10.ws0	regular	8.0	on	0	on
11.ws-	regular	8.0	on	-10^{-3}	on
12.ws+	regular	8.0	on	4×10^{-3}	on
13.s-	regular	0	on	-10^{-3}	off
14.ws+	regular	8.0	on	4×10^{-3}	off
15.s-	group	0	on	-10^{-3}	on
16.ws+	group	8.0	on	4×10^{-3}	on

2.4. Results

For case notation: '0', '-', and '+' corresponds to neutral, negative, and positive buoyancy of particles, respectively; 's' means sinking behavior is included; and 'w' is onshore wind is included (Table 2.1).

2.4.1. No wind case

Particles in Cases 1.0, 3.+, and 6.s+ do not reach the surf zone (Fig. 2.3). Particles in Cases 2.- and 4.s0 partially entered the surf zone, while particles in Case 5.s- are dominant within the surf zone (Fig. 2.3). The negatively buoyant particles with sinking

behavior stay closer to the bottom than ones without the sinking behavior (Fig. 2.4A). Relatively large number of particles stay on offshore bottom longer (Fig. 2.4A) because the particle releasing location is there and bed current (streaming) offshore is weaker than close-shore (Fig. 2.4B).

In the no wind case, vertical profiles of cross-shore velocity consistently show onshore currents near the bed at x = 125 m and farther offshore (Fig. 2.4B). Note that the rip and shoal velocities in Fig. 2.4B are alongshore- and time-averaged velocities of all defined rip channels and shoals. The averaging masks episodic strong rip current velocities (Reniers et al. 2010). Within the surf zone (at x = 75 and 100 m), the Eulerian velocities show offshore currents, however, by adding Stokes drift (= Lagrangian velocity), bottom flow changed to onshore, while the surface current is still offshore, except on the shoal at x = 75 m where Lagrangian velocities are onshore throughout the water column.

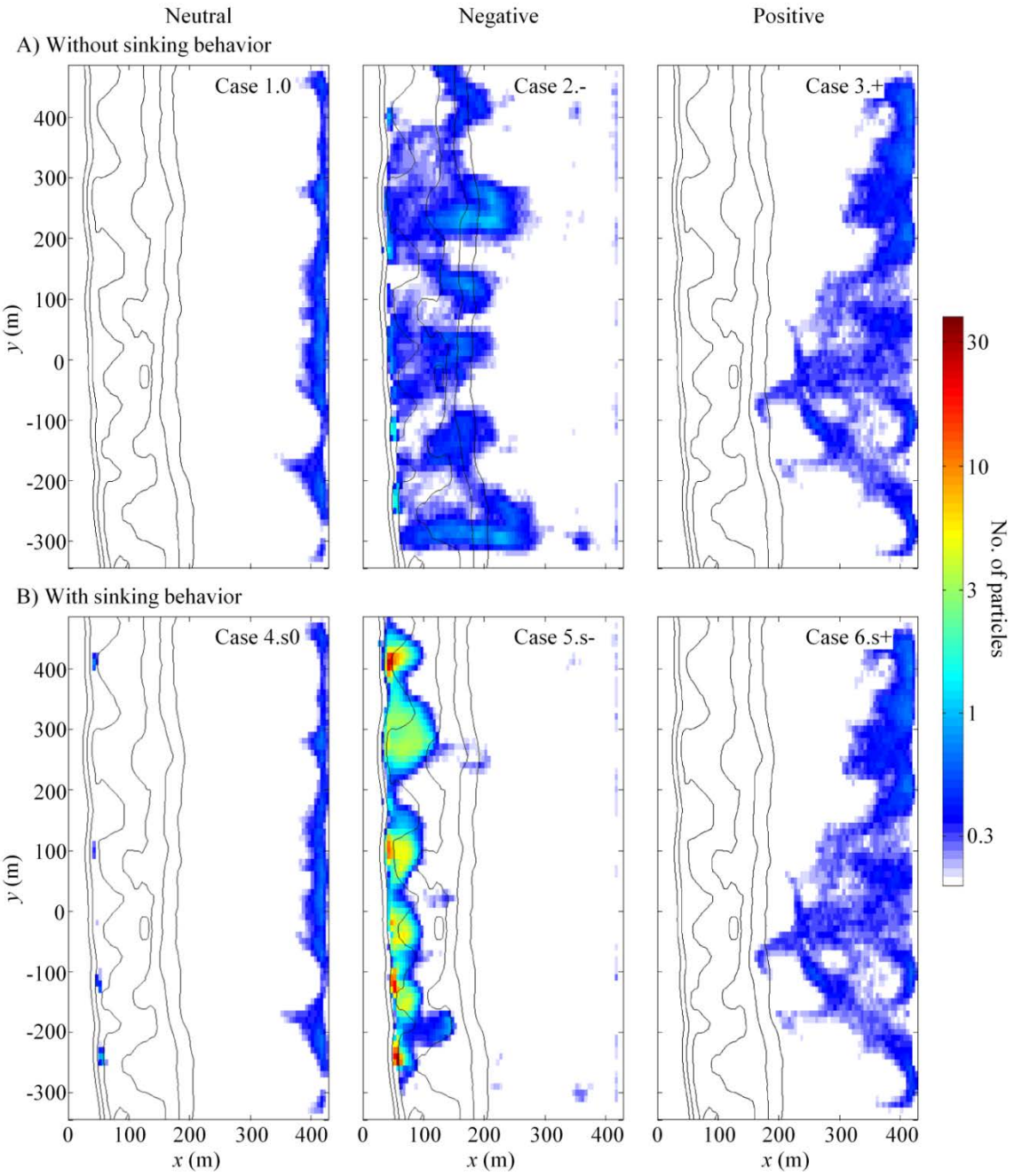

Fig. 2.3. Depth- and time-averaged number of particles per grid cell. Regular wave, no wind, Stokes drift, with buoyancy of neutral (Cases 1.0 and 4.s0), negative (Cases 2.- and 5.s-), and positive (Cases 3.+ and 6.s+). (A) Particles without sinking behavior, and (B) with sinking behavior. Bottom contour lines from 0 m depth (shore line) to 5 m depth with 1 m increments are given. The color bar is in a log scale.

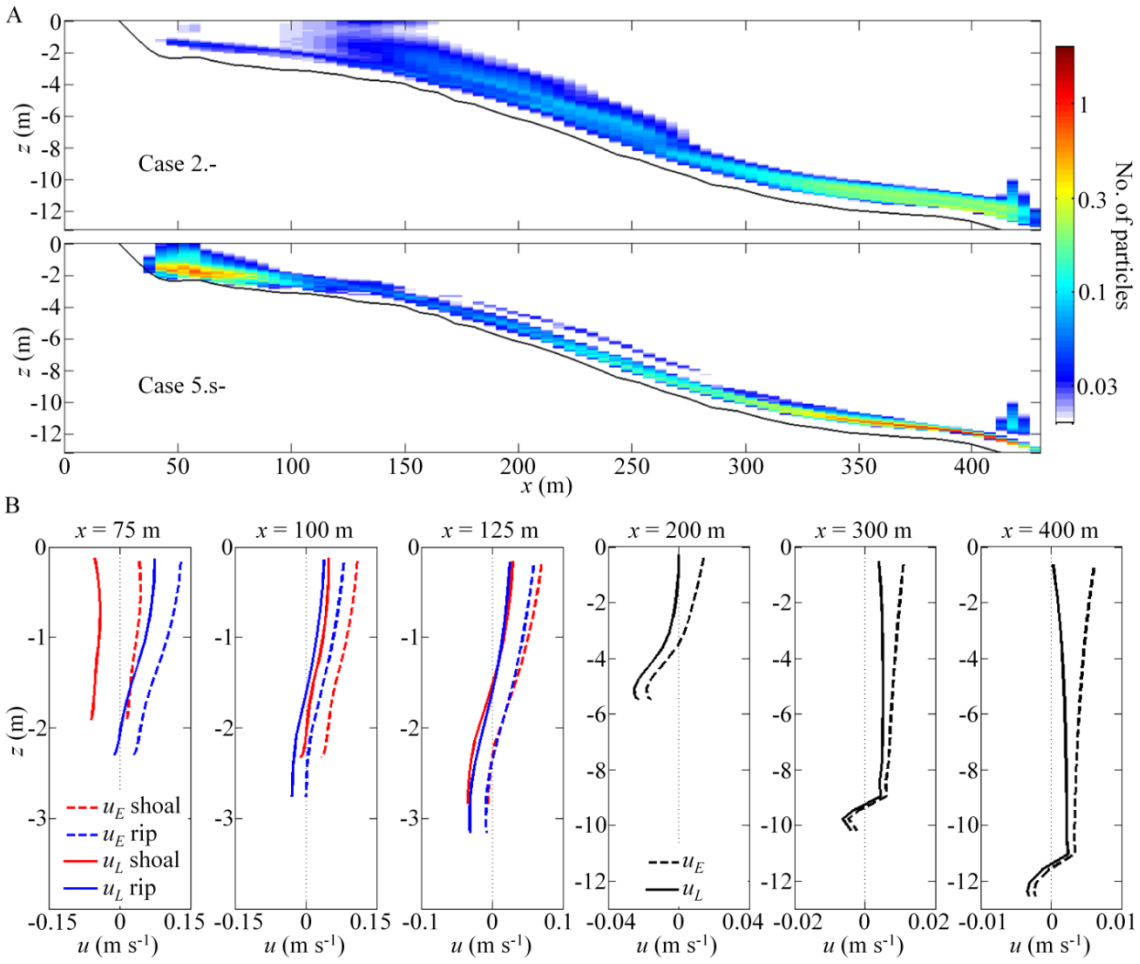

Fig. 2.4. (A) Alongshore- and time-averaged number of particles per grid cell. Regular wave, no wind, Stokes drift, negative buoyancy, without sinking behavior (Case 2.-) and with sinking behavior (Case 5.s-). The maximum depth line is shown as a bottom frame. The color bar is in a log scale. (B) Vertical profiles of alongshore- and time-averaged cross-shore velocities in the physical model case of regular waves without wind. Dashed line is Eulerian velocity (u_E) and solid line is Lagrangian velocity (u_L). The first three panels to the left are average velocities in the rip channels (blue) and on the shoals (red), and the others are averages over the total alongshore ranges (black). Positive values correspond to offshore currents.

2.4.2. Onshore wind case

Particles in Cases 7.w0, 8.w-, and 11.ws- do not reach the surf zone (Fig. 2.5). Particles in Cases 9.w+ and 10.ws0 partially cross the surf zone, while those in Case 12.ws+ are dominant in the surf zone (Fig. 2.5). The positively buoyant particles are near the surface in Case 9.w+ and outside of the surf zone in Case 12.ws+. The particles with sinking behavior sink in the surf zone (Fig. 2.6A).

Wind forcing alters the cross-shore velocity vertical profiles (Fig. 2.6B). Again, these velocities are alongshore- and time-averaged velocities. Streaming is suppressed and surface water flows toward shore at x = 200, 300, and 400 m. Like the no wind case, at x = 75, 100, and 125 m the Eulerian velocity shows an offshore current, however, the Lagrangian velocity near the bed changes to an onshore current, while the surface current still flows offshore in the rip at x = 75 and 100 m and on the shoal at x = 125 m. Lagrangian velocities in the entire water column at x = 75 m are onshore.

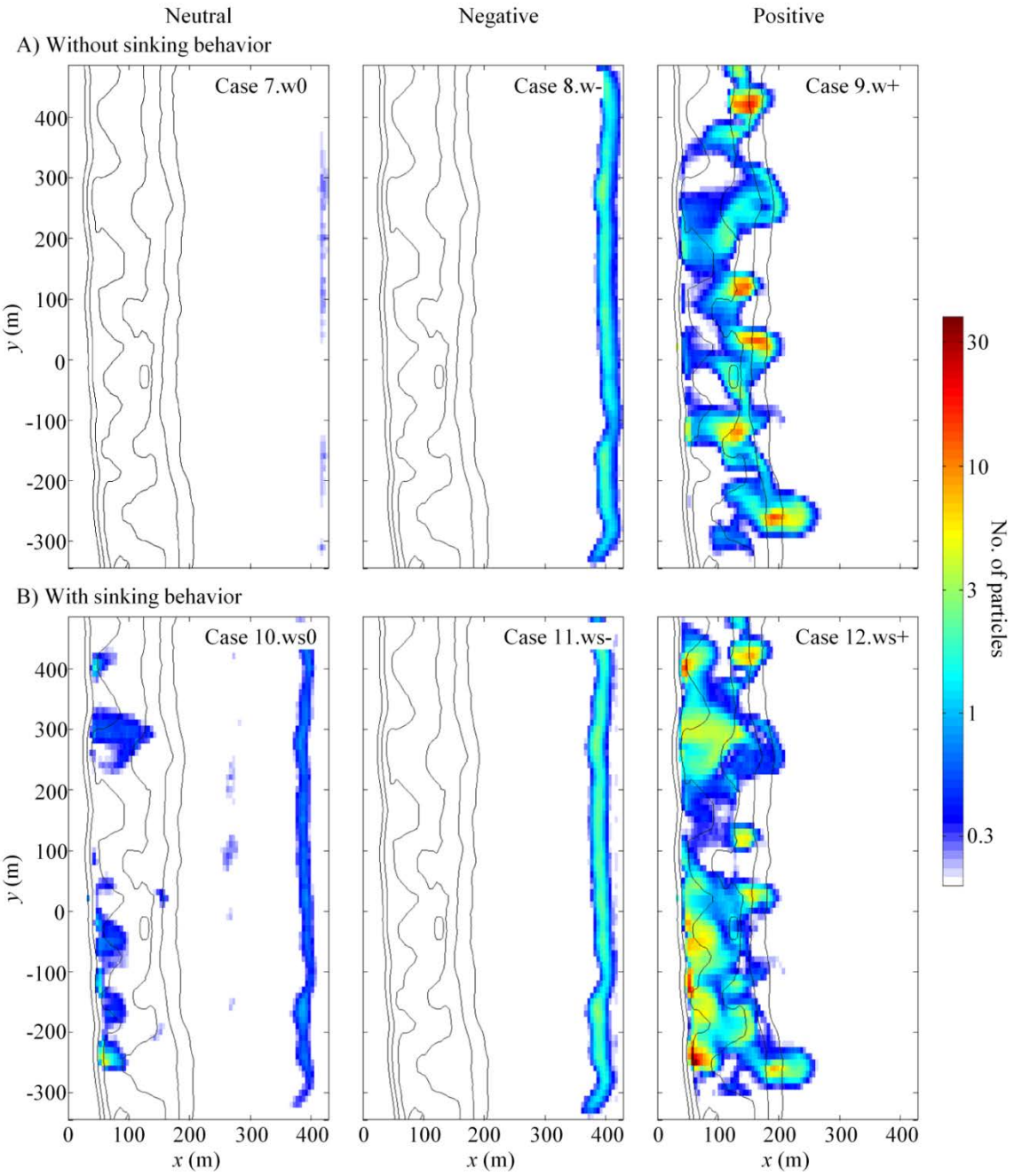

Fig. 2.5. Depth- and time-averaged number of particles per grid cell. Regular wave, wind, Stokes drift, with buoyancy of neutral (Cases 7.w0 and 10.ws0), negative (Cases 8.w- and 11.ws-), and positive (Cases 9.w+ and 12.ws+). (A) Particles without sinking behavior, and (B) with sinking behavior. Bottom contour lines from 0 m depth (shore line) to 5 m depth with 1 m increments are given. The color bar is in a log scale.

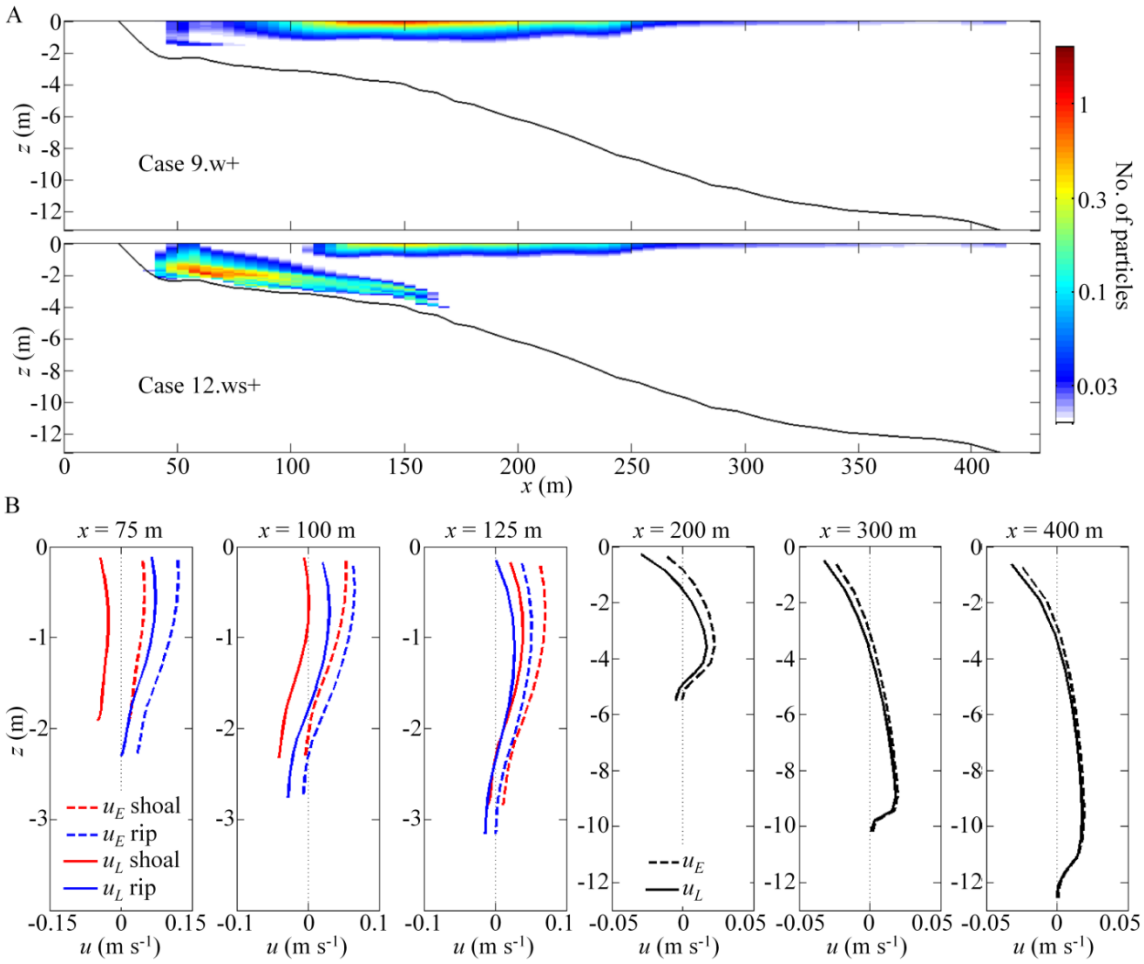

Fig. 2.6. (A) Alongshore- and time-averaged number of particles per grid cell. Regular wave, wind, Stokes drift, positive buoyancy, without sinking behavior (Case 9.w+) and with sinking behavior (Case 12.ws+). The maximum depth line is shown as a bottom frame. The color bar is in a log scale. (B) Vertical profiles of alongshore- and time-averaged cross-shore velocities in the physical model case of regular waves with wind. Dashed line is Eulerian velocity (u_E) and solid line is Lagrangian velocity (u_L). The first three panels to the left are average velocities in the rip channels (blue) and on the shoals (red), and the others are averages over the total alongshore ranges (black). Positive values correspond to offshore currents.

2.4.3. Cases with high onshore migration rate

Cases 5.s- (Regular waves, no wind, Stokes drift, negative buoyant particles with the sinking behavior) and 12.ws+ (Regular waves, wind, Stokes drift, positive buoyant particles with the sinking behavior) are two scenarios in which particles successfully migrated to the shore by crossing the surf zone. 17% and 12% of entire particles exit from the alongshore outlets in Cases 5.s- and 12.ws+, respectively, so these cases in Figs. 2.3 and 2.5 represent most particles. The following subsections show other characteristics of these cases, and corresponding cases with different physical parameters.

2.4.4. Effects of Stokes drift and wave group

When Stokes drift is not included, most particles that are able to cross the surf zone barrier in Cases 5.s- and 12.ws+ are not able to enter the surf zone in Cases 13.s- and 14.ws+, respectively (Fig. 2.7A).

Random wave group forcing alters the patterns of particle distributions (Fig. 2.7B). Particles in Case 5.s- and 12.ws+ are approximately evenly distributed in rip channels, however, those with wave groups (i.e., Cases 15.s- and 16.ws+, respectively) are patchier. Rip ejections can be seen at the head of rip channels ($x = 200 \pm 30$ m) in Case 16.ws+.

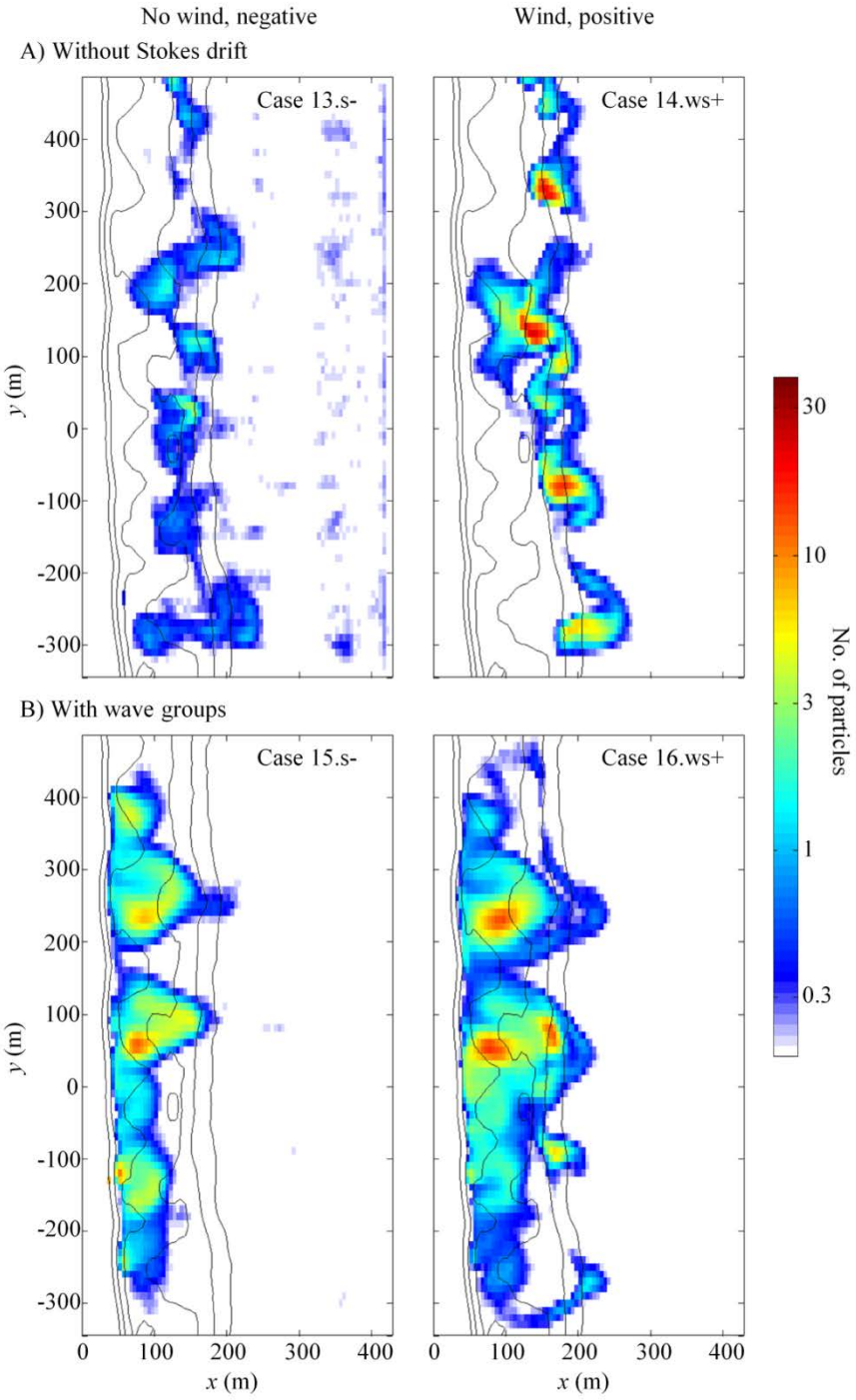

Fig. 2.7. (A) Depth- and time-averaged number of particles per grid cell in cases with sinking behavior, (A) regular wave, without Stokes drift, and (B) wave groups, with Stokes drift. No wind, negative buoyancy (Case 13.s-, Case 15.s-). Wind, positive buoyancy (Case 14.ws+, Case 16.ws+). These cases correspond to Cases 5.s- and 12.ws+, respectively. Bottom contour lines from 0 m depth (shore line) to 5 m depth with 1 m increments are given. The color bar is in a log scale.

2.5. Discussion

Our model study shows both physical forcing (i.e., waves and currents) and biological processes (i.e., vertical position within the water column and sinking in turbulence) may play important roles in the onshore migration of larvae. Although it is theoretical, the model results give an idea of how larval behavior, which is hard to demonstrate and observe in the field, may affect the entrance of larvae into the surf zone.

To enter the surf zone from offshore, larvae need to have the sinking behavior described by Fuchs et al. (2004). Recent studies revealed turbulence-induced downward movement can be seen in other intertidal invertebrates (Roy et al. 2012, Fuchs et al. 2013), so this behavior seems to be common in many intertidal larvae. In addition to vertical movement, horizontal swimming, which I ignore because I focus on the importance of vertical motions of weak swimmers, could also help for the cross-shore migration by relatively strong swimmers such as fish and crab larvae. Staaterman et al. (2012) showed the significance of horizontal swimming for larval settlement by using a similar biophysical model scheme. The horizontal swimming direction might be determined by sound (Vermeij et al. 2010), sunlight (Shanks 1995), chemical signals (Paris et al. 2013*a*) and other environmental stimuli (reviewed by Kingsford et al. 2002). These orientation behaviors should be the subject of future studies to better understand how strongly swimming larvae may cross the surf zone.

Stokes drift appears to be essential for larvae to enter the surf zone, and the model results are consistent with the computational drifter results reported by Reniers et al. (2009). By including Stokes drift the cross-shore velocities near the bed at the approximate edge of the surf zone (x = 100 m) and at x = 125 m both with and without

wind as well as in rip channels at x = 75m in no-wind case, where the most larvae sink due to the high turbulence, are changed from offshore directed to onshore (Figs. 2.4B, 2.6B). Cross-shore transport rates change with wave conditions as it affects Stokes drift, wave breaking and surf zone eddies as well as the general rip-current circulation and as such will be important in explaining daily variability in larval concentrations.

Shear stress exerted by the wind alters the velocity profiles considerably. Current directions are offshore near the surface and onshore near the bottom (i.e., streaming) in the no wind conditions, which is consistent with the model by Lentz et al. (2008). Larvae present near the bottom may be carried toward shore by streaming. The same flow pattern should be observed under offshore wind event. With onshore wind forcing, current directions become onshore near the surface and offshore near the bottom in the offshore area, and similar patterns were observed by Fewings et al. (2008). Thus, the surface flow generated by wind stress may help surface-dwelling larvae move onshore, however, the model suggests that it inhibits the onshore movement of larvae residing near the bottom.

When larvae keep floating without sinking behavior in the wind case, they tend to stack around the surf zone edge (x = 125 m) where the surface current is the result from a delicate balance between the offshore-directed mass-flux and the onshore forcing by the wind (Fig. 2.6). The mass flux builds up to the outer edge of the surf zone, and is compensated over a decreasing depth, resulting in an increasing offshore velocity towards the surf zone edge. In addition, due to the intermittent breaking at the surf zone edge, the turbulent eddy viscosity at the surface is enhanced compared to further offshore, resulting in a weaker vertical shear. These two effects combined result in an offshore directed flow at the surf zone edge. This transition from onshore to offshore-directed surface currents in

the presence of wind is not site specific, but does depend on the wave and wind conditions.

Given the model results that larvae entering the surf zone need turbulence-dependent sinking behavior, Stokes drift, and combinations of vertical positions (i.e., larval buoyancy) and wind-dependent cross-shore flow, there are two possible scenarios, which may generate cross-shore larval migration. In one scenario, negatively buoyant (or downward swimming) larvae migrate onshore without wind stress (Fig. 2.8A). Larvae sink and are kept in the turbulent bottom boundary layer, where turbulence is high enough to induce the sinking behavior. In the boundary layer, larvae are carried by streaming into the surf zone. In the other model scenario, positively buoyant (or upward swimming) larvae migrate from offshore under wind forcing (Fig. 2.8B). Larvae drift at or near the water surface until they reach the edge of the surf zone where turbulence is high enough to induce larvae to sink thereby avoiding offshore flow near the surface and enhancing onshore transport near the bottom. In the model with wind (Case 12.ws+), some buoyant particles are entrained by eddies in the rip-head zone around x = 150 m, and stayed at the surface (Fig. 2.8B). Floating particles trapped by this type of eddies are also shown by Reniers et al. (2010).

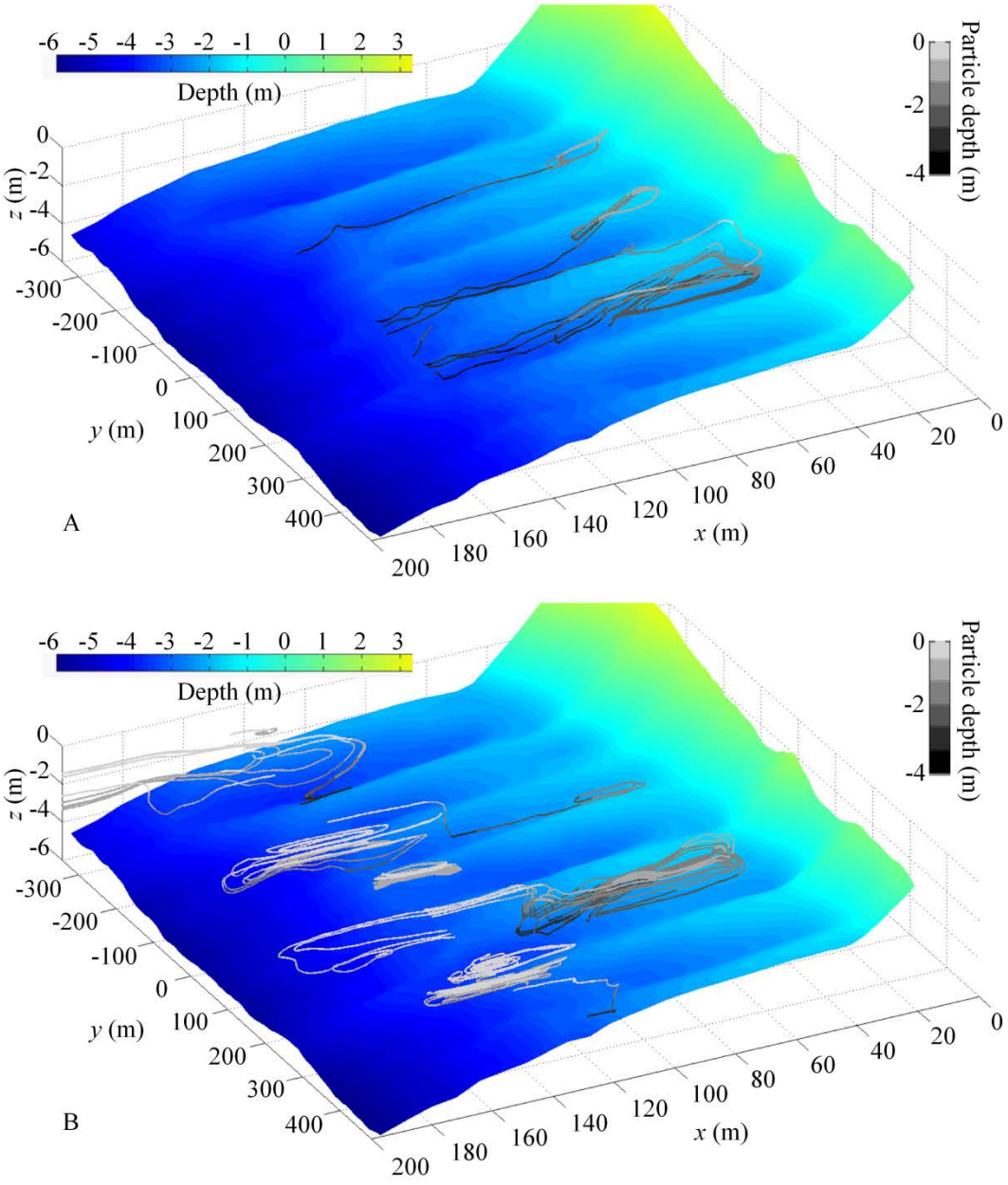

Fig. 2.8. Example of particle pathways in (A) Case 5s- and (B) Case 12.ws+.

In a horizontal view, particles near the bottom generally are transported over the shoals first, and then typically converge in the rip channels by locally circulating (Figs. 2.9 and 2.10). After the particles enter the rip, they are carried toward the surface by upward flow and transported away from shore by return flow (Fig. 2.8). Once the return flow forcing becomes small, they sink again and are carried shoreward again by the bed flow, resulting in persistent circulation patterns (Fig. 2.8). This mechanism is unique to a rip-channeled beach with predominantly normally incident waves.

In the successful migration scenarios, the concentrations of modeled particles in rip channels are higher than on shoals and offshore (Fig. 2.11A). This is consistent with larval concentrations documented in the field (Fig. 2.11B, $p < 0.05$). Whether physical factors, such as tides and changing wave conditions, affect these concentrations is not considered here. Because the model results are based on vertical velocities of competent gastropod larvae (Fuchs et al. 2004), specific density, vertical velocities and swimming behaviors of other species probably also need to be concerned to provide a species-specific model for onshore transport of larvae across the surf zone. Nevertheless, there seems to be common factor(s), such as sinking behavior, affecting patch distributions of zooplankton across taxa because statistical analysis shows that concentrations of all three taxa, including copepods as holoplankton, in the rip are significantly higher than on the shoal and offshore ($p < 0.05$), and there is no significant difference between concentrations on the shoal and offshore ($p > 0.05$) (Fig. 2.9B). Quantified data from the successful migration model cases support the observed higher concentration of competent larvae in the surf zone compared with offshore (Table 2.2).

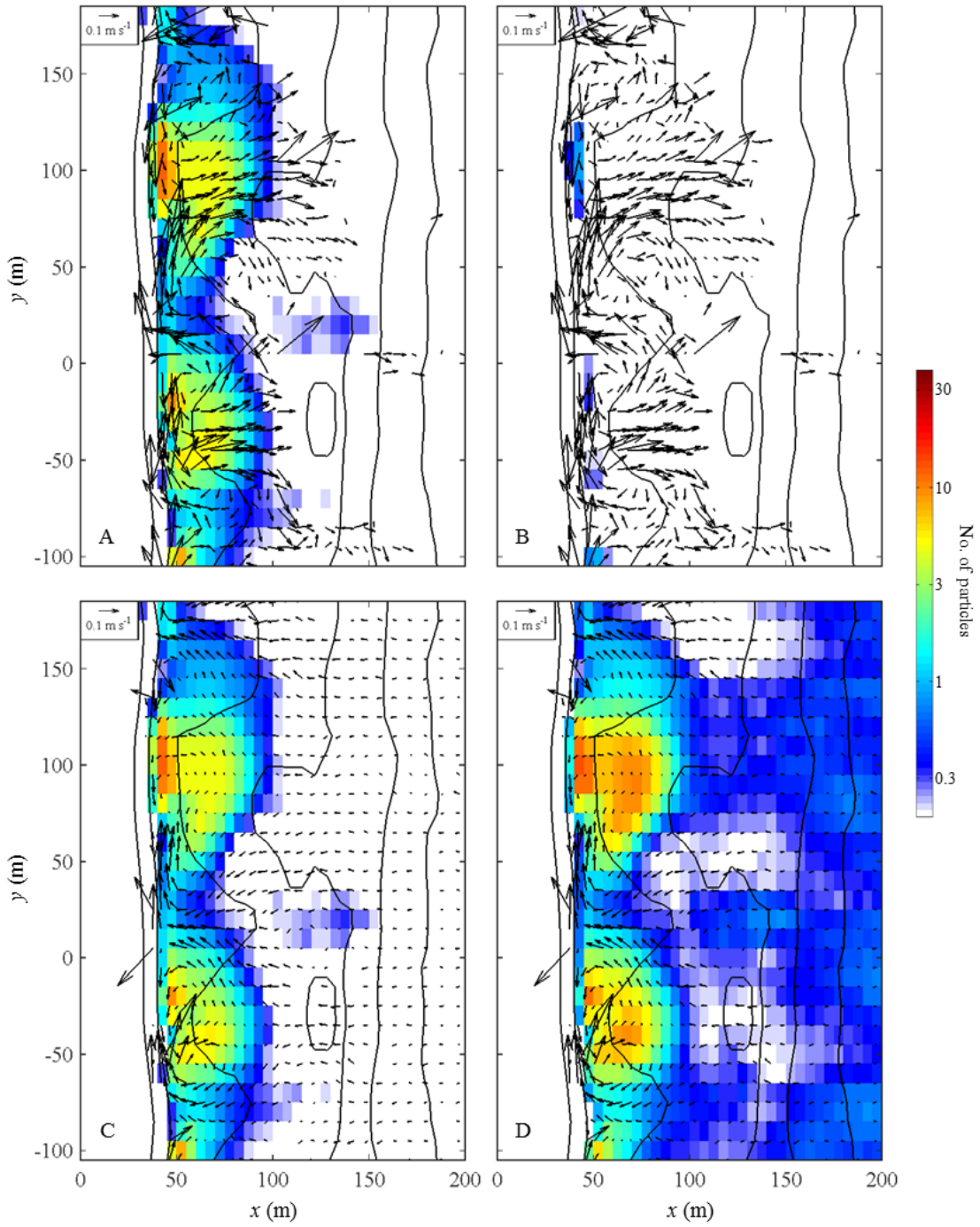

Fig. 2.9. Time-averaged horizontal velocity vectors in Case 5.s-. Contour lines from 0 m depth (shore line) to 3 m depth with 1 m increment are given. (A) Particle velocities (Lagrangian velocities and motions of particles) on the surface overlaid with depth- and time-averaged number of particles. (B) Particle velocities on the surface overlaid with time-averaged number of particles integrated 0.25 m depth and above. (C) Particle velocities on the bed overlain with depth- and time-averaged number of particles. (D) Particle velocities on the bed overlain with and time-averaged number of particles integrated 0.25 m from the bed and below.

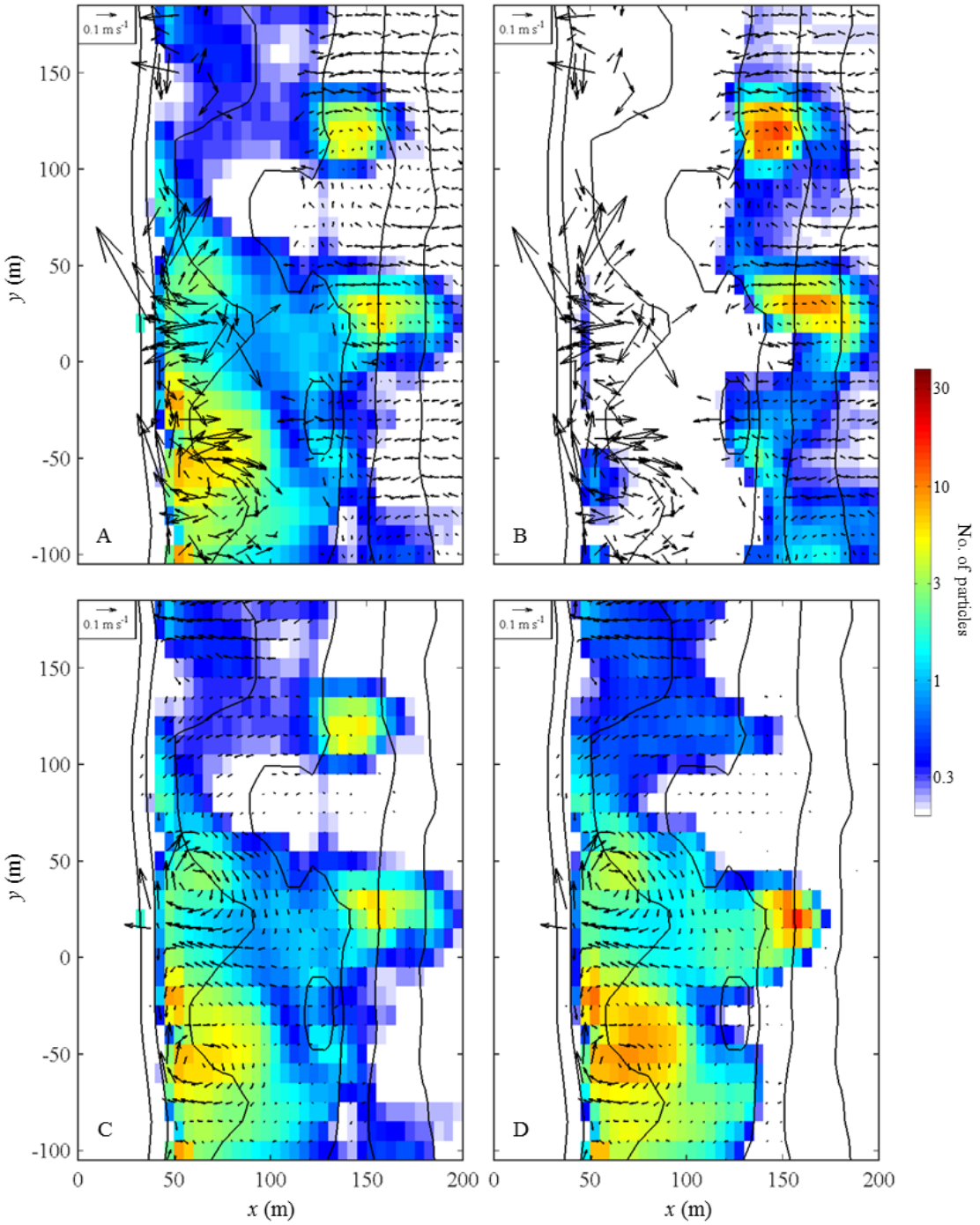

Fig. 2.10. Time-averaged horizontal velocity vectors in Case 12.ws+. Contour lines from 0 m depth (shore line) to 3 m depth with 1 m increment are given. (A) Particle velocities (Lagrangian velocities and motions of particles) on the surface overlaid with depth- and time-averaged number of particles. (B) Particle velocities on the surface overlaid with time-averaged number of particles integrated 0.25 m depth and above. (C) Particle velocities on the bed overlain with depth- and time-averaged number of particles. (D) Particle velocities on the bed overlain with and time-averaged number of particles integrated 0.25 m from the bed and below.

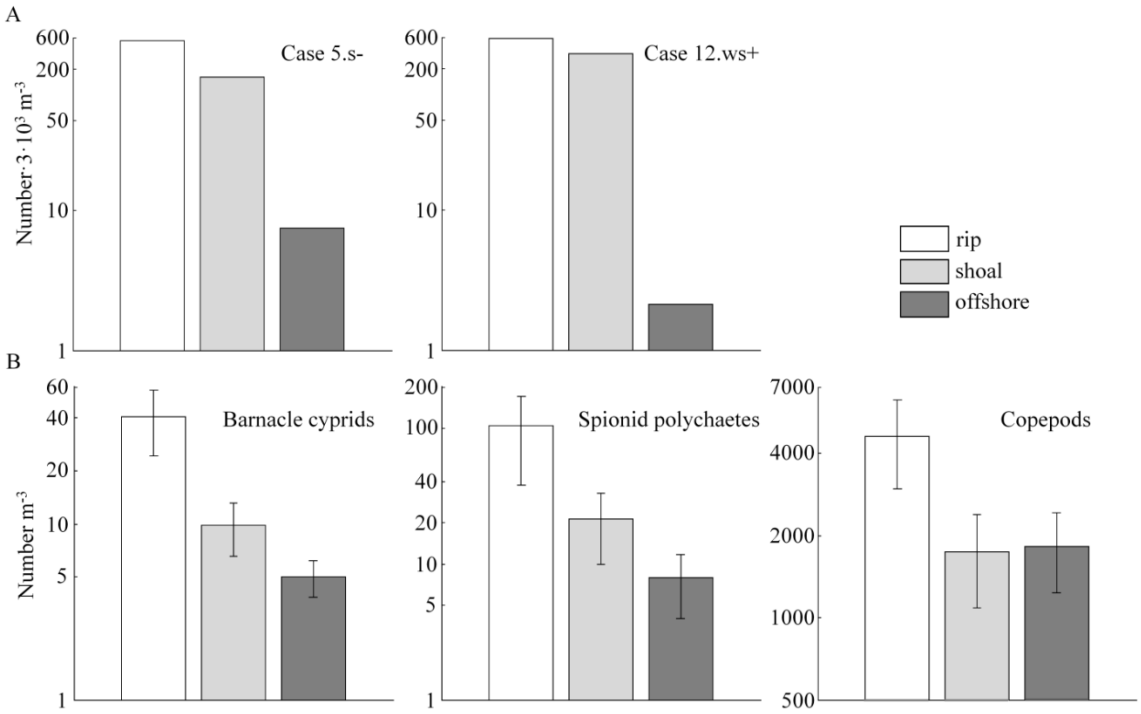

Fig. 2.11. (A) Time-averaged number of particles per m^3 in the rip channels ($x < 100$ m), on the shoals ($x < 100$ m), and offshore ($x > 200$ m), in cases with regular wave, sinking behavior, Stokes drift. No wind, negative buoyancy (Case 5.s-). Wind, positive buoyancy (Case 12.ws+). (B) Average concentrations (± 95% confidence interval) of barnacle cyprids, spionid polychaetes, and copepods in the rip channel, on the shoal, and offshore in the field.

Table 2.2. Ratios of particles in the rip to offshore and particles on the shoal to offshore. The ratios in the model cases are calculated for depth-averaged and depth-integrated particles.

Model case or taxon	Rip:Offshore	Shoal:Offshore
5.s- (depth-averaged)	67.7	19.8
5.s- (depth-integrated)	17.8	3.1
12.ws+ (depth-averaged)	153.1	88.2
12.ws+ (depth-integrated)	40.3	13.9
Barnacle cyprid	11.8	2.3
Spionid polychaete	25.8	2.7
Copepod	3.2	1.6

The locations and sizes of larval patches in the wave group cases (Fig. 2.7B) differ from those in the regular wave cases (Cases 5.s- and 12.ws+ in Figs. 2.3B and 2.5B, respectively). The patches in the wave group cases are larger and concentrated at fewer locations. Although the distribution patterns differ, all of these cases achieved onshore larval transport, and resulted in higher larval concentrations in the rip channels than on the shoals, as was observed in the field results (Fig. 2.9).

That floating particles exit from the surf zone through rip currents is more clearly seen in Case 16.ws+ than that in Case 12.ws+. This is likely a result of the generation of surf zone eddies by the incident wave groups that can temporarily trap particles. Once these eddies detach from the rip circulation, they can eject the particles offshore forming narrow surface streaks outside of the surf zone (Reniers et al. 2010), as shown in Fig. 2.7B.

For longer time scales, tidal forcing also may affect larval transport (Shanks 1986, Pineda 1999). At least timing of onshore migration could be determined by the tides. Along with the tidal cycle, diurnal wind stresses are important for long-term cross-shore transport of water, as found by Hendrickson and MacMahan (2009). Larvae residing near the bottom are transported shoreward during wind relaxation or offshore wind events, whereas larvae residing near the surface are transported shoreward during onshore wind events. Fewings et al. (2008) showed that alongshore winds do not substantially contribute to cross-shore exchange near shore and, in addition, alongshore winds were weak during the sampling period.

Although this model is simplified, it provided two reasonable scenarios of larval transport across the surf zone at a rip-channeled beach. Of course, the mechanisms

applied in this study are not exhaustive and the model can be developed with additional environmental conditions. In particular, the transport within the breaking wave roller might be of importance as mentioned earlier. The model results are representative for rip-channeled beaches only. And although this is a specific beach type, it is very common in nature. The modeled wave and flow patterns within the surf zone are consistent with literature on rip-channeled beaches (Wright & Short 1984, Dalrymple et al. 2011), and outside of the surf zone the modeled flow patterns are also consistent with other studies (Fewings et al. 2008, Lentz et al. 2008). However, the surf zone circulation is affected by the bathymetry and it is worth testing with other types of beaches.

Chapter 3

TRANSPORT OF LARVAE AND DETRITUS AT A STEEP POCKET BEACH

3.1. Introductory Remarks

Processes of larval delivery to shores may vary with beach morphology. The previous chapter showed possible mechanisms of larval transport at the gentle sloping beach with rip channels. Here I examine the effects of physical, biological, and morphological factors on the delivery of competent larvae to the surf zone at Carmel River State Beach (CRSB), characterized as a steep pocket beach, by using a biophysical numerical model based on Chapter 2.

An accompanied field study showed that competent larvae and detritus were frequently more concentrated in the surf zone than offshore, while holoplankton and precompetent larvae were found much less in the surf zone than offshore (Shanks et al. 2015). Since concentration of detritus was significantly correlated with concentrations of competent larvae in the surf zone at CRSB, there is probably a common mechanism of onshore delivery of detritus and competent larvae at this beach, thus transport of detritus is simulated here as well. The study also revealed that concentrations of detritus and competent larvae within the surf zone were negatively correlated with wave height. Hence I also examine the effect of wave height on these concentrations.

3.2. Field Survey

Physical data were collected at CRSB (36^{o} 32’18” N; 121^{o} 55’43” W), CA in the summer of 2011 (Fig. 3.1A). CRSB is a steep pocket beach with typically a very narrow surf zone of $O(10)$ m. Current and wave data were obtained by acoustic Doppler current

profilers (ADCPs). Bathymetric data used for the model simulations were collected with a personal water craft and kayak equipped with an echo sounder and a Global Positioning System (GPS). The dry beach and inter-tidal areas were mapped by a walking person carrying a GPS backpack. There is a lagoon behind the beach and the river mouth was closed most of the time during the survey period, and the presence of the ephemeral river is ignored in the model.

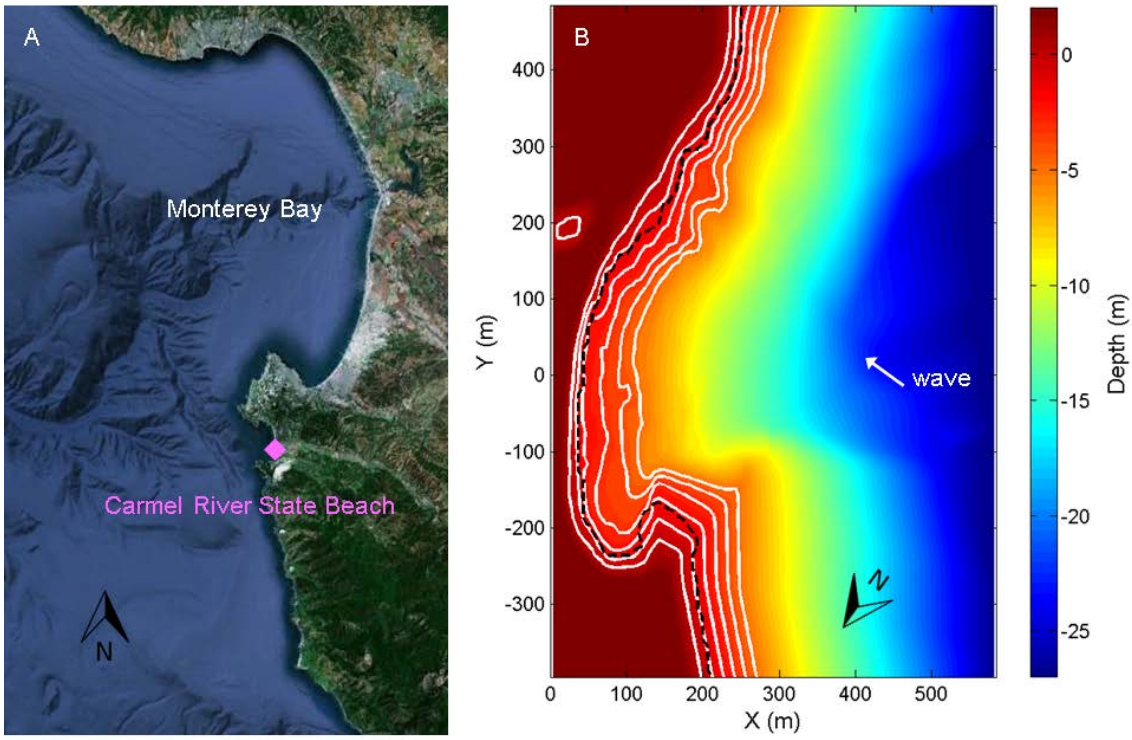

Fig. 3.1. (A) The locations of Carmel River State Beach (CRSB) (Credit: Google Earth). (B) Bathymetry at CRSB. White bottom contour lines are in 1 m increments from depth of 0 m (shoreline) to 5 m. Black dashed line is the approximate surf zone edge as a reference. The modeled wave angle obtained from time-averaged field data is indicated by the white arrow.

3.3. Numerical Simulations

3.3.1. Hydrodynamic model

Similarly to Chapter 2, waves and currents are calculated by Delft3D. The model domain spans 1050 m in the alongshore direction, 600 m in the cross-shore direction, and the depth is based on the collected bathymetry data (Fig. 3.1B). Note that north points toward the bottom (offshore to the right) due to the coordinate system. The beach profile at Y = 0 m, where the ADCPs were deployed, consists of a 1/7.6 subaerial beach slope, 1/3 subaqueous beach step, and 1/19 subaqueous beach profile. The model mesh scheme is a regular grid (hexahedral cells) with grid spacing of 10 m along the beach, approximately 5–10 m in the cross-shore with the finest spacing at the shoreline, and 14 σ-layers representing the depth with a fine mesh near the bed in order to resolve bottom boundary layer streaming. Cross-shore reflections are controlled by an offshore Riemann boundary, which is a weakly-reflective open boundary, and alongshore reflections are suppressed by a weakly-reflective water level boundary to the south, while the north side is a closed boundary. In the analysis I cut off 50 m of the northern and 100 m of the southern end in order to eliminate potentially adversely affected boundary currents. A k-ε closure scheme is used for modeling turbulence. Oblique waves with 0.4 m root-mean-square wave height (H_{rms}) and 9.45 s peak wave period, based on the average wave data during the survey period in the summer of 2011, are generated at the offshore boundary. Wave angles did not vary widely during the survey period, so the time-averaged wave angle ($\theta = 36°$) is used (Fig. 3.1B). In addition, a H_{rms} of 0.2 m and 0.8 m corresponding to approximately the lowest and the highest H_{rms} observed during the field survey, respectively, are also applied in order to investigate the effect of wave height on

concentrations of detritus and larvae in the surf zone. Imposing either no wind or 8.0 m s^{-1} constant onshore wind tests the effect of wind stress.

The model is idealized to show a typical larval transport pattern at CRSB using the same settings as used in Chapter 2. The duration of a model run is 2 h with a time step of 3 s and an output interval of 6 s. Diurnal events, such as tides and diurnal wind are not considered here, so the 2-h simulation output is used periodically for a 24-h larval transport simulation.

3.3.2. Larval transport model

An individual based model with the same Lagrangian transport equations as the ones used in Chapter 2 is applied. For all the simulations presented here, Stokes drift is included, which plays a critical role in the delivery of larvae to the surf zone as shown by the model in the previous chapter. The earlier model also suggests that another essential part of the transport mechanism is turbulence-dependent sinking behavior, where competent larvae stop swimming and sink to the bottom at -10^{-2} m s^{-1} by their own body weight when the turbulent energy dissipation rate is greater than 10^{-5} m^2 s^{-3} (Fuchs et al. 2004). Note that turbulent dissipation rates exceeding this threshold occur almost everywhere in the surf zone and within the bottom boundary layer.

Each individual particle is assigned a vertical velocity (w) either -10^{-3} m s^{-1} or 4×10^{-3} m s^{-1}, which represents buoyancy or vertical swimming speed of a competent larva as used in Chapter 2, or -2.5×10^{-3} m s^{-1}, the average sinking velocity of detritus (Shanks et al. 2015). No active horizontal swimming behavior is considered here. In the 24-h simulation time, 637 particles equally distributed alongshore (ΔY = 10 m) are released every hour from offshore (X = 550 m) or closer to the shore (X = 350 m), and also from

north (Y = -390 m) equally distributed cross-shore (ΔX = 2.5 m) at two vertical locations for two types of particles: near the bottom for the particles with negative buoyancy (detritus and bottom dwelling larvae); and near the water surface for the ones with positive buoyancy (floating larvae). Offshore and lateral sides are considered to be outlet boundaries, i.e., once a particle gets out of the model domain, it is not taken into account any more. The first 12-h run is used as a spin-up stage for particle initialization, and only the simulation from 12 h to 24 h is used to calculate the time-averaged number of particles per grid cell. The model cases and parameters are summarized in Table 3.1: Each case name describes a test condition: 'W' if onshore wind is included; 'S' if sinking behavior is included; '-', '+', and 'D' corresponds to negatively and positively buoyant larvae, and negatively buoyant detritus, respectively. For example, Case 1.S- is negatively buoyant larvae with sinking behavior are released during no wind event.

3.4. Results

3.4.1. No wind case

Depth- and time-averaged particle concentrations for the no wind case are shown in Fig. 3.2. Particles released at X = 550 m (Cases 1.S-, 2.S+, 3.-, and 4.D) collected in patches outside the surf zone but mostly do not enter the surf zone. Some particles released at X = 350 m (Cases 5.S-, 6.S+, 7.-, and 8.D) reach the surf zone, but their distributions are very patchy. These high density particle patches in the surf zone tend to be in the south rather than at the northern end of the surf zone.

The difference of particle concentrations between two different initial release locations (X = 550 m and 350 m) indicates differences in cross-shore flow patterns between offshore and near the surf zone. This also suggests that the influx of particles

from the lateral boundaries may be important. In fact, some particles released at Y = -390 m are carried by an alongshore current (Fig. 3.3I-L). However, high concentrations of sinking particles in the south (> Y = 200 m) in Cases 5.S-, 7.-, and 8.D may be mainly due to cross-shore current and streaming (see Fig. 3.4 as an example) although it is unclear how the particles arrive at the initial location X = 350 m.

Water flow entrains in the cove around (X, Y) = (100 m, -200 m), and continue as an alongshore current up to about Y = 150 m (Fig. 3.3) consistent with dye observations at the same location (Brown et al. in review). The alongshore current is separated from shore and formed an eddy at (X, Y) = (300 m, 150 m). There is a relationship between the particle patch distributions of Cases 5.S- and the bottom current pattern rather than the surface current as expected for sinking particles (Fig. 3.3). Particles trapped by eddies result in high concentration patches. Some particle patch locations are common among the model cases (Fig. 3.2) correlated with underlying flow patterns (Fig. 3.3). A notable feature is the recirculation at about (X, Y) = (300 m, 150 m), where each case has a relatively high concentration. Another common high concentration spot is at (X, Y) = (50 m, -50 m) which is between the shoreline and the alongshore current and coincides with the presence of an eddy that trapped particles.

3.4.2. Onshore wind case

Fig. 3.5 shows the depth- and time-averaged particle densities for the onshore wind case at CRSB. Negatively buoyant particles with sinking behavior and detritus released at X = 550 m and 350 m (Cases 13.WS-, 16.WD, 17.WS-, and 20.WD) do not enter the surf zone because the wind driven surface currents alter the bottom currents from onshore to offshore (Fig. 3.6A), and are thus flushed offshore. A small amount of

these particles released at Y = -390 m (Cases 21.WS- and 24.WD) enter the surf zone in the north.

A relatively large patch is commonly observed at (X, Y) = (200 m, 200 m) in cases with positively buoyant particles both with sinking behavior and without sinking behavior released at X = 550 m (Case 14.WS+ and Case 15.W+) and X = 350 m (Case 18.WS+ and Case 19.W+). This patch is related to the eddy at the same location (Fig. 3.6). Particle pathways illustrate this eddy-derived patch very well (Fig. 3.7).

Sinking behavior may not be important for floating particles to settle. Unlike negatively buoyant particles in the no-wind case, positively buoyant particles probably reach the surf zone better without sinking behavior. This is mainly because the alongshore current carries more floating particles (Case 23.W+) than sinking particles (Case 22.WS+). Positively buoyant particles with sinking behavior tend to be dispersed and stayed in the north (Fig. 3.5J). However, particle concentrations in the south (> Y = 250 m), as seen in Cases14.WS+, 15.W+, 18.WS+, and 19.W+, seem to be forced by cross-shore currents (Fig. 3.6).

Similarly to the no wind case, water flow entrains in the cove first, and forms an alongshore current, then the current is separated from shore and forms an eddy at (X, Y) = (300 m, 100 m) (Fig. 3.6). The consistent alongshore current in both wind cases was also observed in the field survey at CRSB (Brown et al. in review).

Table 3.1. Model cases at CRSB. "Wind" is either no wind (no) or onshore wind (yes) = 8.0 m s^{-1}. "Release location" is initial cross-shore (X) or alongshore (Y) position of particles. "Sinking" is turbulence-dependent sinking behavior of larvae, included (on) or not (off). "*w*" is vertical velocity of particles. Each case name describes a test condition: "W" if onshore wind is included; "S" if the sinking behavior is included; "+" and "-" correspond to positive and negative buoyancy of larvae, respectively, and "D" is detritus, which is also negatively buoyant.

Case	Wind	Release location	Sinking	w ($\times 10^{-3}$ m s^{-1})
1.S-	no	X = 550 m	on	-1.0
2.S+	no	X = 550 m	on	4.0
3.-	no	X = 550 m	off	-1.0
4.D	no	X = 550 m	off	-2.5
5.S-	no	X = 350 m	on	-1.0
6.S+	no	X = 350 m	on	4.0
7.-	no	X = 350 m	off	-1.0
8.D	no	X = 350 m	off	-2.5
9.S-	no	Y = -390 m	on	-1.0
10.S+	no	Y = -390 m	on	4.0
11.-	no	Y = -390 m	off	-1.0
12.D	no	Y = -390 m	off	-2.5
13.WS-	yes	X = 550 m	on	-1.0
14.WS+	yes	X = 550 m	on	4.0
15.W+	yes	X = 550 m	off	4.0
16.WD	yes	X = 550 m	off	-2.5
17.WS-	yes	X = 350 m	on	-1.0
18.WS+	yes	X = 350 m	on	4.0
19.W+	yes	X = 350 m	off	4.0
20.WD	yes	X = 350 m	off	-2.5
21.WS-	yes	Y = -390 m	on	-1.0
22.WS+	yes	Y = -390 m	on	4.0
23.W+	yes	Y = -390 m	off	4.0
24.WD	yes	Y = -390 m	off	-2.5

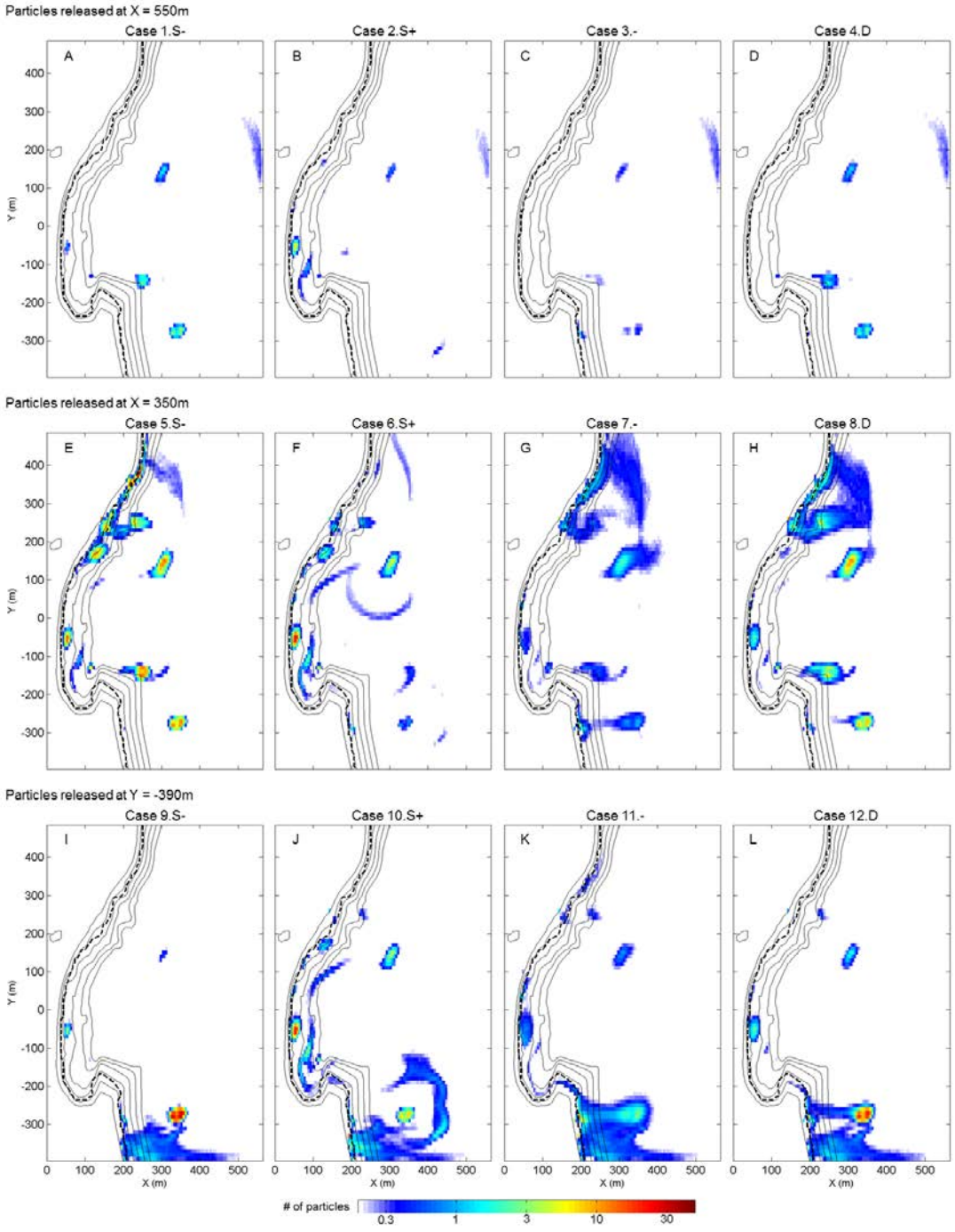

Fig. 3.2. Depth- and time-averaged number of particles per grid cell in no wind case. Initial cross-shore particle release positions are (A, B, C, D) X = 550 m, (E, F, G, H) X = 350 m, and (I, J, K, L) Y = -390 m. (A, E, I) Negatively buoyant particles with sinking behavior. (B, F, J) Positively buoyant particles with sinking behavior. (C, G, K) Negatively buoyant particles without sinking behavior. (D, H, L) Detritus. Bottom contour lines from 0 m depth (shore line) to 5 m depth with 1 m increments are given as a reference. Black dashed lines are the approximate surf zone edges.

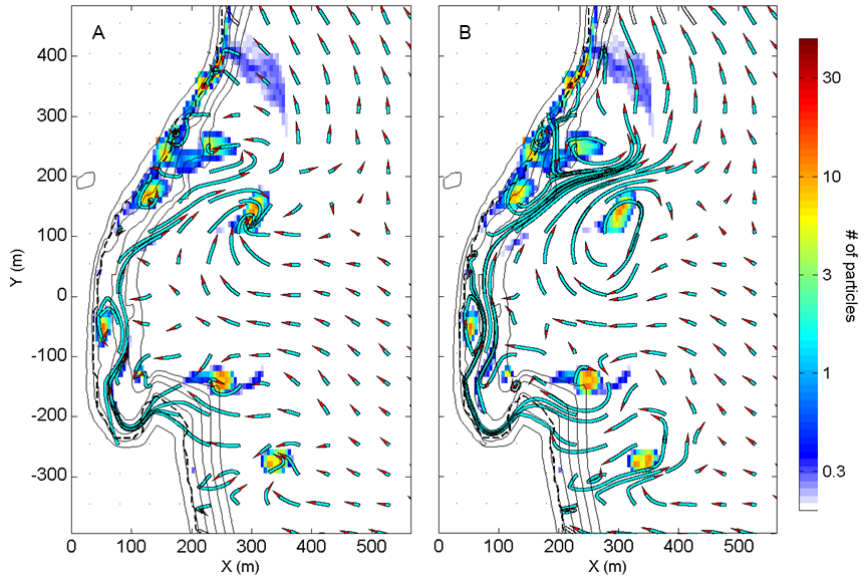

Fig. 3.3. Trajectories of Lagrangian velocities in no wind condition (A) at the bottom and (B) at the surface with an integration interval of 30 min. Velocity direction is indicated by a red tip. Overlay color map is time and depth-averaged number of particles in Case 5.S-. Approximate surf zone edge is indicated by a dashed line. Bottom contour lines from 0 m (shore line) to 5 m with 1 m increments are given.

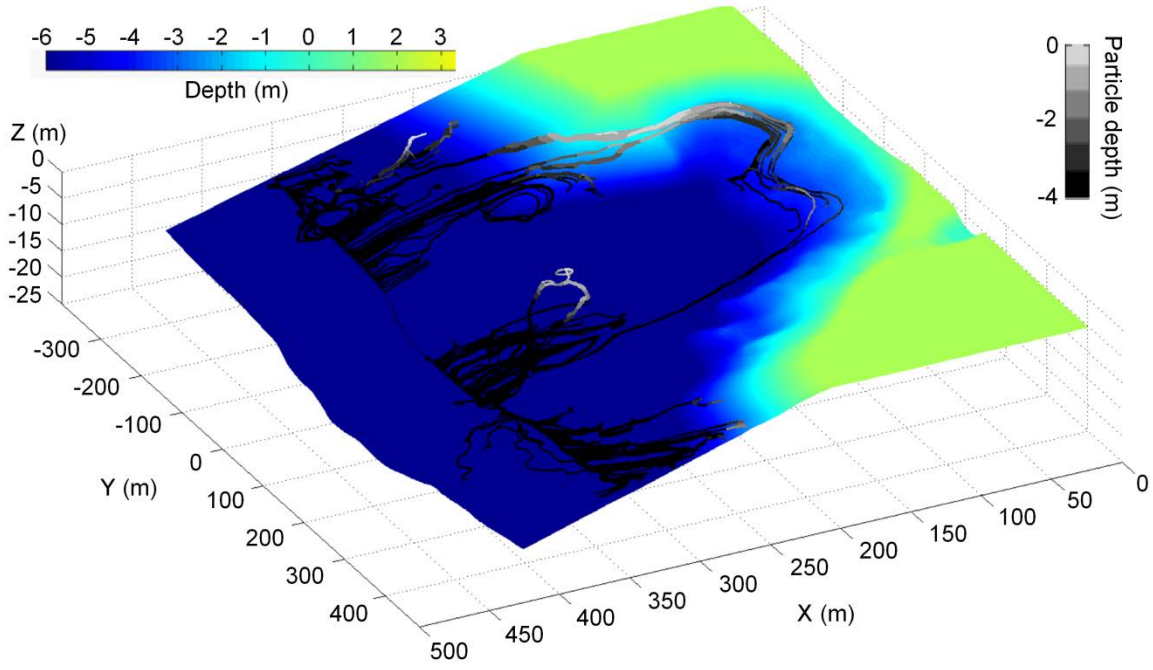

Fig. 3.4. Example of particle pathways in Case 5.S-.

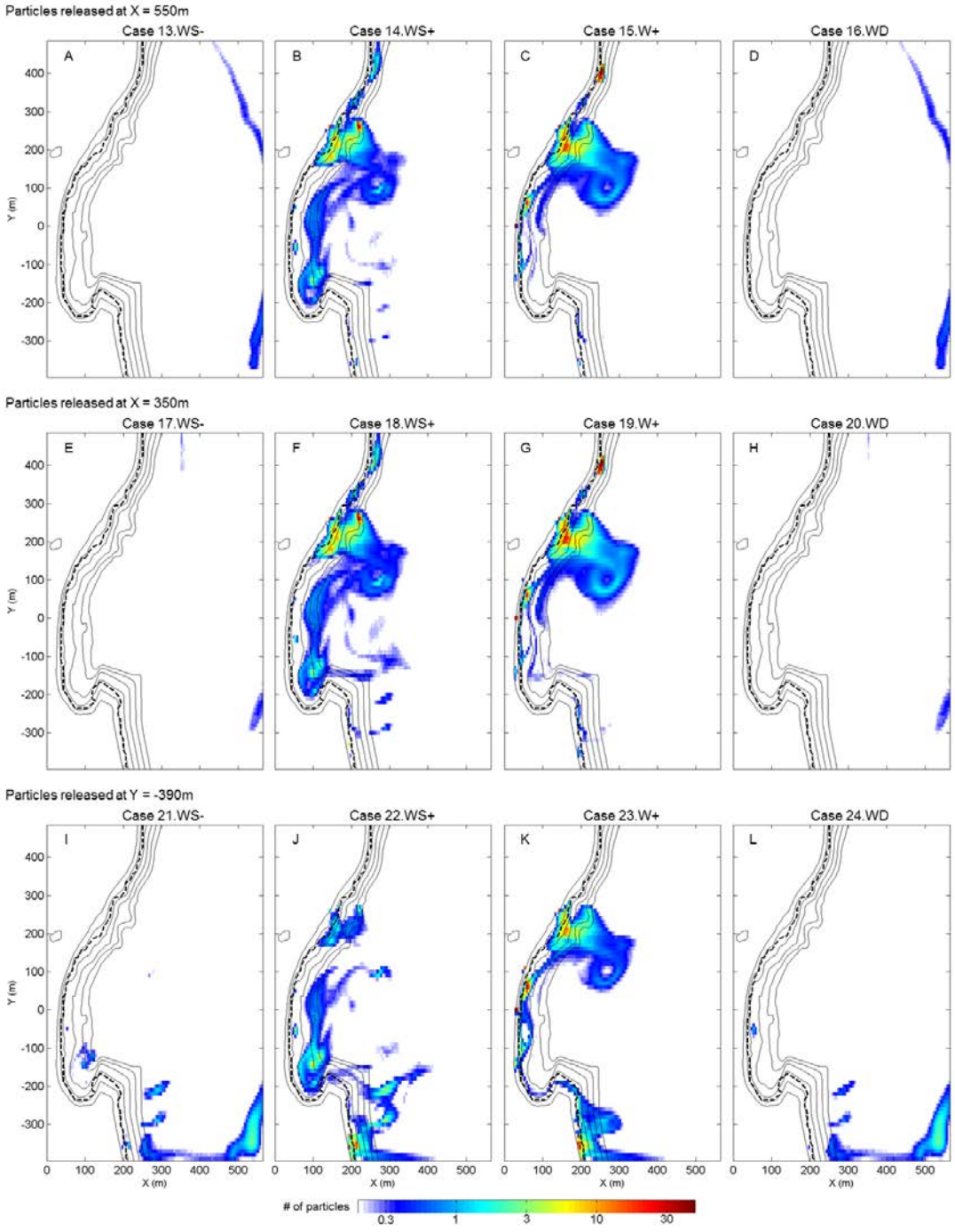

Fig. 3.5. Depth- and time-averaged number of particles per grid cell in onshore wind case. Initial cross-shore particle release positions are (A, B, C, D) X = 550 m, (E, F, G, H) X = 350 m, and (I, J, K, L) Y = -390 m. (A, E, I) Negatively buoyant particles with sinking behavior. (B, F, J) Positively buoyant particles with sinking behavior. (C, G, K) Positively buoyant particles without sinking behavior. (D, H, L) Detritus. Bottom contour lines from 0 m depth (shore line) to 5 m depth with 1 m increments are given as a reference. Black dashed lines are the approximate surf zone edges.

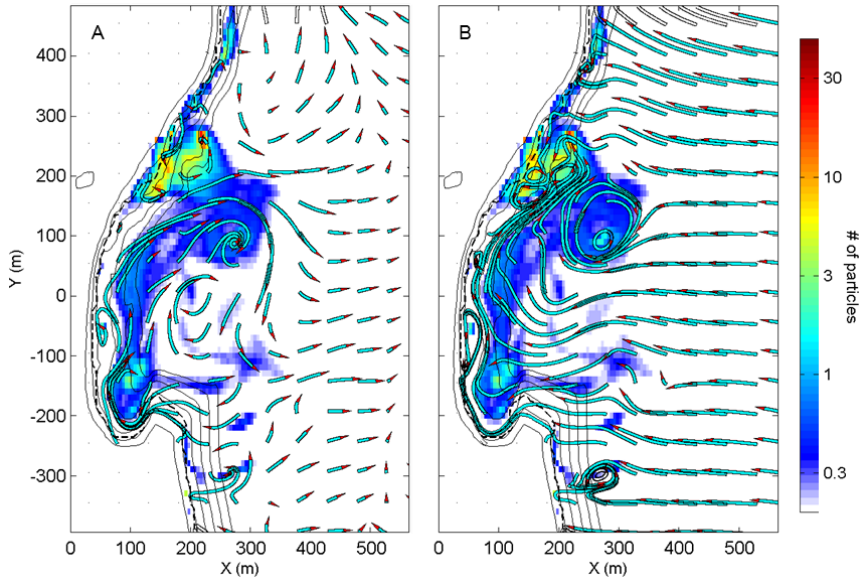

Fig. 3.6. Trajectories of Lagrangian velocities in onshore wind condition (A) at the bottom and (B) at the surface with an integration interval of 30 min. Velocity direction is indicated by a red tip. Overlay color map is time and depth-averaged number of particles in Case 18.WS+. Approximate surf zone edge is indicated by a dashed line. Bottom contour lines from 0 m (shore line) to 5 m with 1 m increments are given.

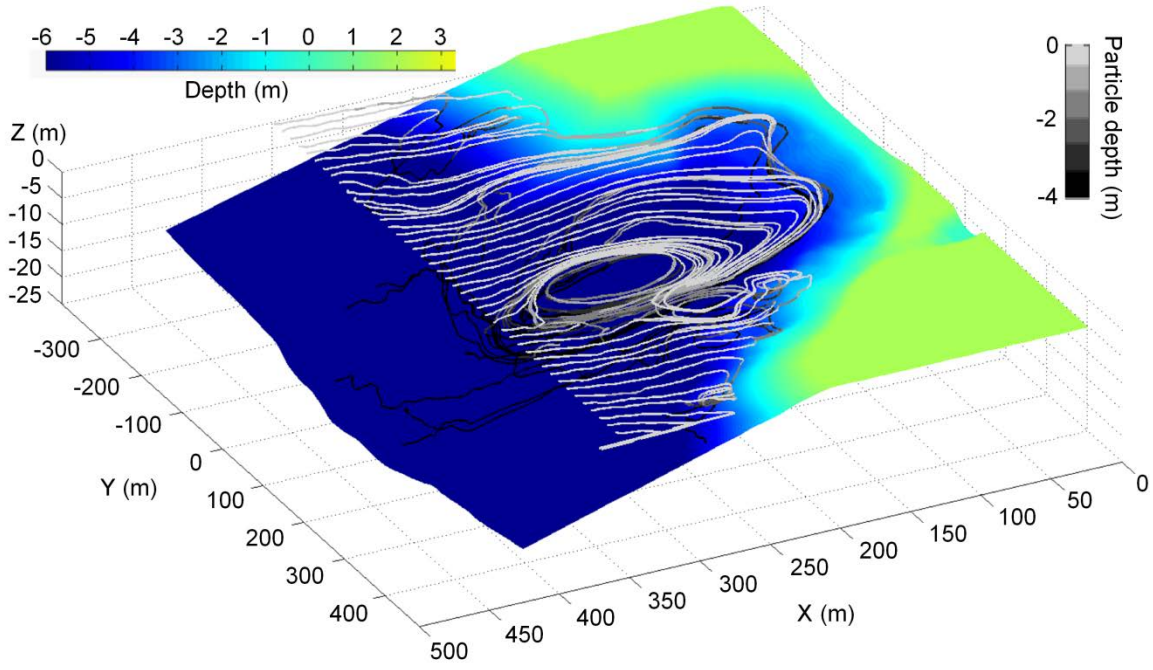

Fig. 3.7. Example of particle pathways in Case 18.WS+.

3.4.3. Effect of wave height

Lower and higher wave heights are applied to the cases that represent successful onshore transport patterns (Fig. 3.8). Note that width of surf zone got narrower and wider as the surf zone wave height became smaller with H_{rms} = 0.2 m and larger with H_{rms} = 0.8 m, respectively. Currents are weak and a few small eddies are formed very close to the shore in the case with H_{rms} = 0.2 m, that leads to relatively high concentrations of particles in the surf zone (Fig. 3.9A, B). Higher waves (H_{rms} = 0.8 m) produce stronger currents that flush most of the particles out of the domain through the southern boundary (Fig. 3.9C, D).

Adding onshore wind change the flow patterns as some eddies can be seen outside the surf zone, and the alongshore current seen in the medium wave height case (Fig. 3.3) reverses direction (Fig. 3.9B) because wave induced currents for H_{rms} = 0.2 m are too small, and wind driven currents thus control the current pattern. Evidently the effect of onshore wind on the currents is smaller in the high wave case than the other cases.

Concentrations of modeled larvae (Cases 5.S- and 18.WS+) and detritus (Case 8.D) in the surf zone with the alongshore range of Y = ±100 m are negatively correlated with wave height (Fig. 3.10). This is consistent with Shanks et al. (2015) whose sampling site was at about (X, Y) = (50 m, 0 m).

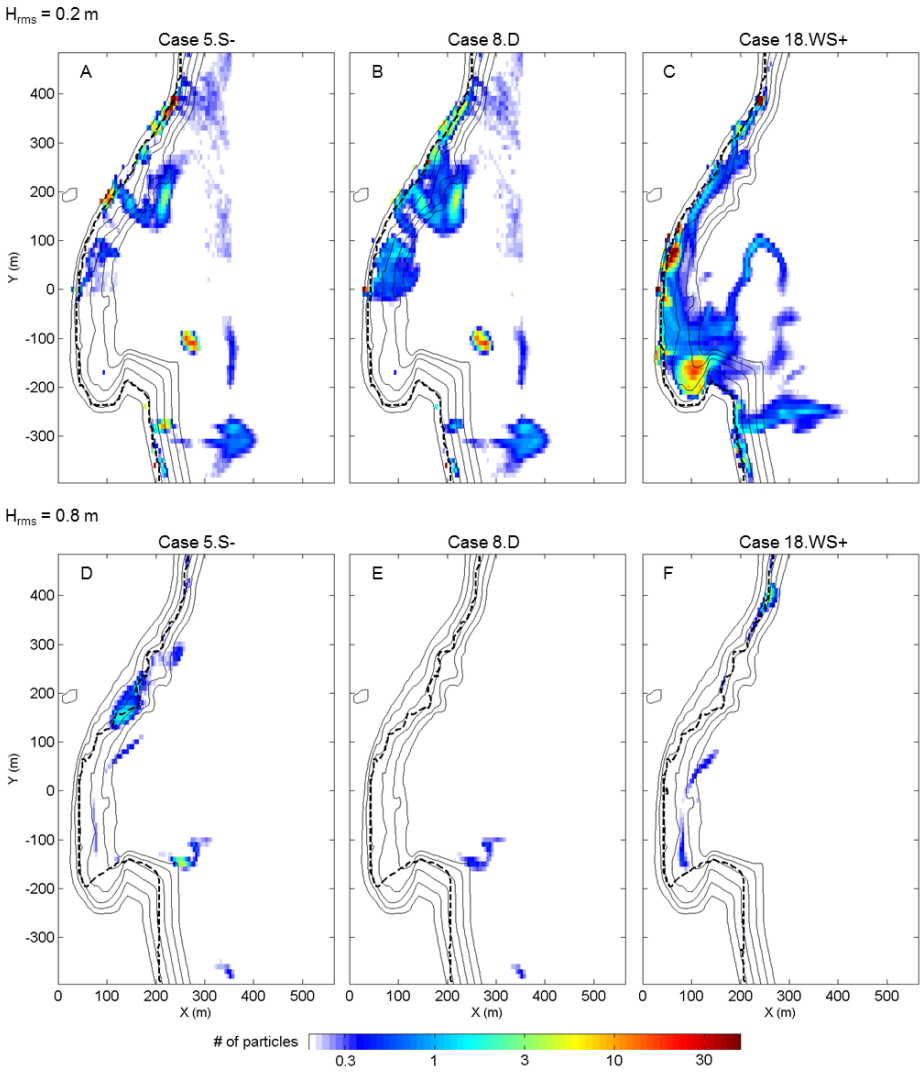

Fig. 3.8. Subcases of Cases 5.S-, 8.D, and 18.WS+. (A, B, C) H_{rms} = 0.2 m, (D, E, F) H_{rms} = 0.8 m. Note that the approximate surf zone edge indicated by a black dashed line changed with wave height.

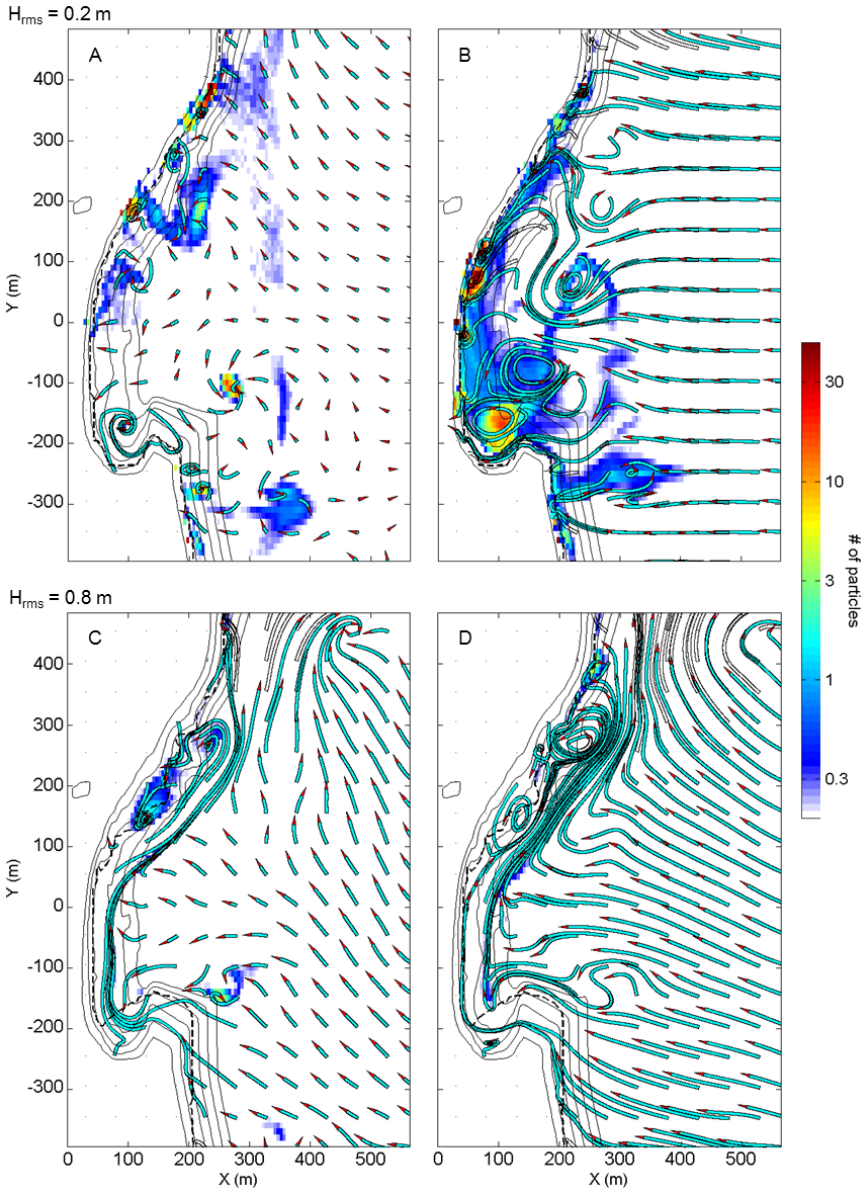

Fig. 3.9. Trajectories of Lagrangian velocities in onshore wind condition (A, C) at the bottom and (B, D) at the surface with an integration interval of 30 min. Velocity direction is indicated by a red tip. Overlay color map is time and depth-averaged number of particles in subcases of (A, C) Case 5.S- and (B, D) Case 18.WS+ with (A, B) H_{rms} = 0.2 m, (C, D) H_{rms} = 0.8 m. Approximate surf zone edge is indicated by a dashed line. Bottom contour lines from 0 m (shore line) to 5 m with 1 m increments are given.

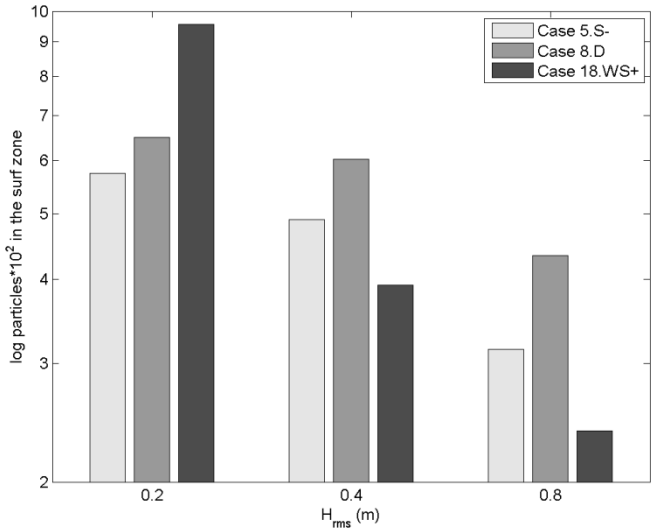

Fig. 3.10. Time-averaged number of particles in the surf zone with the alongshore range of Y = ±100 m in three H_{rms} subcases.

3.5. Discussion

The concentration of detritus is correlated with the concentration of negatively buoyant particles, and this is also consistent with the field study (Shanks et al. 2015). Detritus thus can be used as a supplemental tool to track competent larvae (e.g., barnacle cyprids) and detritus-associated organisms (e.g., harpacticoid copepods). Organisms near the surface or in the upper water column probably reach the shore when the onshore wind is strong enough. To investigate further transport and distribution patterns of each taxa, it might be necessary to collect data of vertical distributions of organisms and their characteristics, especially buoyancies, as well as correlations with local wave and wind data.

Smaller wave heights help more competent larvae and detritus to get into the surf zone as the field data show (Shanks et al. 2015) whereas higher waves flush the particles via the strong alongshore current. Note that the settlement of larvae should be more easily

accomplished with smaller waves not only because of the high rate of onshore transport, but also the low energy and turbulence as they need to stick to a substrate.

Other possible factors influencing cross-shore exchange that are not included in the current model are the breaking wave roller and wave reflection. Breaking induced roller can entrain some particles and carry them to the shore, thus contribute to onshore particle transport (Reniers et al. 2013). On the other hand, because wave reflection is high at steep beaches (Battjes 1974), migrating particles might be bounced back offshore due to wave reflection at CRSB as a steep-slope beach. According to the field study by Shanks et al. (2015), approximately 30 % of wave energy reflected offshore in this case, but the reflection does not affect strongly as the observation showed enough onshore currents to transport particles to the surf zone. The model results on particle concentrations are consistent with Shanks et al. (2015), indicating effects of these factors could be minimal in the model cases.

There are common particle transport patterns among cases when particles entered the surf zone for both wind regimes. Particles that reach the southern shore are carried by onshore currents: negatively buoyant particles are delivered by bottom boundary layer streaming; and positively buoyant particles are flowing with the wind driven surface currents. These are similar to the transport mechanisms in the previous model application at Sand City beach. However, particles concentrated on the middle part of the shore are largely affected by the alongshore current. A few near-shore eddies seem to play an important role in forming high particle concentration patches. At the same time, some particles are trapped by several other eddies outside the surf zone.

Effects of particle buoyancy and sinking behavior for ingress into the surf zone at CRSB without wind forcing seem to be less important than in the model cases with the same conditions at a mild sloping rip-channeled beach conducted in Chapter 2. The rate of particles entering the surf zone at CRSB is much lower than that at the mildly sloping rip-channeled beach, and it is consistent with the previous finding that recruitment of intertidal invertebrate larvae is higher at more dissipative than more reflective beaches (Shanks et al. 2010). However, differences between these two beaches are not limited to slopes, but these beaches both have alongshore variability at different scales. CRSB is a pocket beach and the headlands span $O(1000)$ m, whereas Sand City beach has rip channels spacing $O(100)$ m. The complexity of these beaches needs to be decomposed in order to distinctly prove that rates of larval recruitment are higher at more dissipative beaches than steeper beaches.

CRSB is a steep pocket beach with oblique waves, resulting in a southward alongshore current that eventually disconnects from the surf zone to form an offshore flow. This is accompanied by an onshore flow further to the south. Onshore migrating particles initially follow these main currents, then they are trapped by local eddies and eventually make high concentration patches. Smaller eddies are formed closer to the shore with smaller waves, resulting in high larval and detrital concentration in the surf zone; whereas larger waves induce larger and less eddies apart from the surf zone, thus much less larvae and detritus enter or stay in the surf zone.

Chapter 4

EFFECTS OF BEACH SLOPE, ALONGSHORE VARIABILITY, AND WAVE GROUP FORCING ON LARVAL TRANSPORT

4.1. Introductory Remarks

As shown in Chapters 2 and 3, particles released offshore tend to enter the surf zone in greater amount at Sand City beach than at CRSB when the similar physical regimes are applied (Fig. 4.1). Sand city beach is mild sloping rip-channeled beach while CRSB is a steep pocket beach (Fig. 4.2). When one focuses only on beach slopes, the model results indicate that the recruitment rate of competent larvae is higher at more dissipative than more reflective beaches, consistent with Shanks et al. (2010). However, as mentioned in Chapter 3, those two beaches in this study are different in alongshore direction as well: Sand City beach with rip-channels and CRSB with a cove in much larger spatial scale, and how alongshore variability affects larval transport is unclear. Thus, the beach configuration is broken down into simple components. First, alongshore uniform beaches with various slopes are tested with the larval tracking model. Then, rip-channels and shoals are included to see the effect of rip current on cross-shore larval transport. I also test wave group forcing to see if it affects cross-shore exchange as indicated by Reniers et al. (2004).

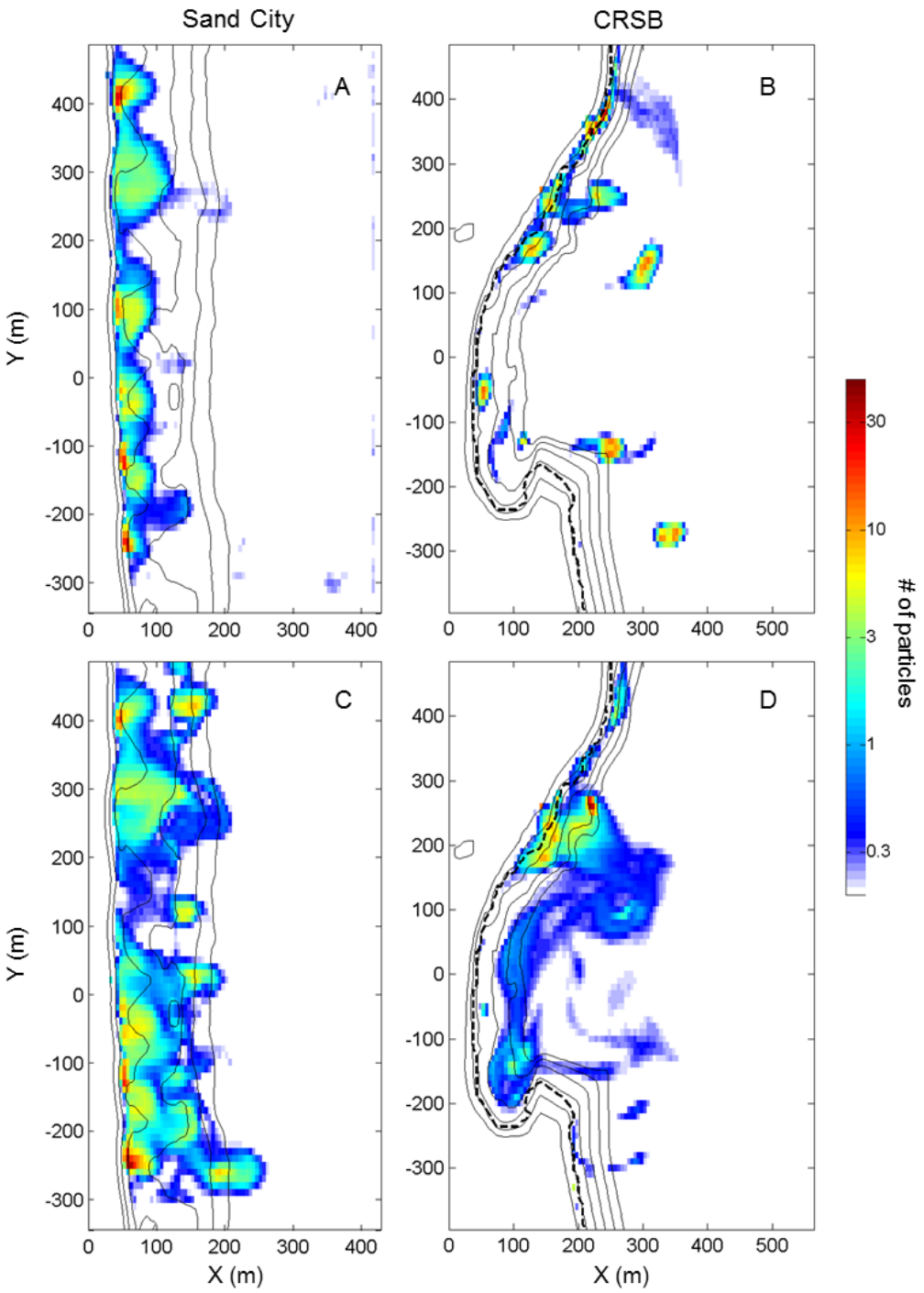

Fig. 4.1. Depth- and time-averaged number of particles per grid cell in (A, B) negatively buoyant particles without wind and (C, D) positively buoyant particles with onshore wind cases at Sand City (A, C) and CRSB (B, D). All the particles have sinking behavior. Bottom contour lines from 0 m depth (shore line) to 5 m depth with 1 m increments are given as a reference. Black dashed lines are the approximate surf zone edges. Corresponding case IDs are (A) 5.s- and (B) 12.ws+ in Chapter 2, (C) 5.S- and (D) 18.WS+ in Chapter 3.

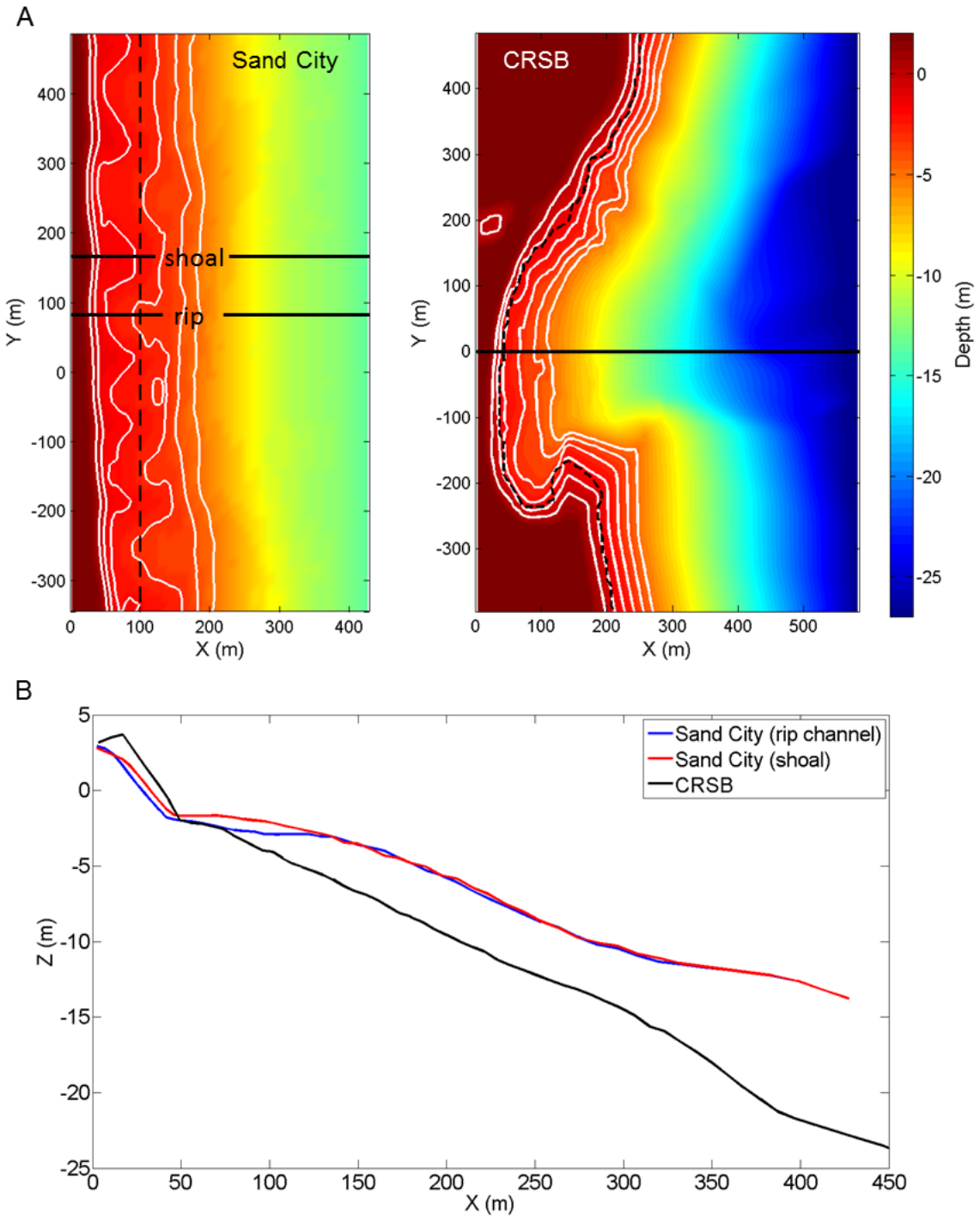

Fig. 4.2. (A) Bathymety at Sand City beach and CRSB. White bottom contour lines are in 1 m increments from depth of 0 m (shoreline) to 5 m. Black dashed lines are the approximate surf zone edges as a reference. Black horizontal lines correspond to (B) beach profiles.

4.2. Methods

Biophysical numerical scheme is presented in Chapter 2. The wave and flow model is calculated by Delft3D. The alongshore length of all the hydrodynamic model domains in this chapter is 1400 m. For alongshore uniform beaches, various constant slopes ranging from 1° to 8° are applied. Based on the alongshore uniform beach with 2° slope, which is about the same degree as the slope of Sand City beach, rip channels and shoals are introduced – a simple alongshore sinusoidal pattern is applied. Rip channel spacing is similar to that of Sand City beach. Bars and the beach face are not included. Additionally, wave group forcing specified with a JONSWAP spectrum (Hasselmann et al. 1973) is introduced into the model case with 2° slope alongshore uniform beach to examine the effect of wave-group induced currents. Maximum offshore depth is 10 m for all cases, thus cross-shore range gets shorter with steeper slopes as shown in Fig. 4.3. The model mesh is composed of hexahedral cells with 10 m constant grid spacing in alongshore direction, approximately 5–10 m in cross-shore direction with the finest spacing at the shoreline, and 14 σ-layers are set in vertically. The grid resolution is higher in the surf zone, and near the bed in order to resolve bottom boundary layer streaming. Water level boundary (weakly-reflective open boundary) is set offshore, and Neumann boundary conditions (water level gradient boundaries) are specified at the alongshore boundaries. Turbulence is simulated by a k-ε model. Normally incident waves with 0.7 m root-mean-square wave height (H_{rms}) and 10 s peak wave period (T_p) are generated at the offshore boundary. Either zero wind stress or 8.0 m s^{-1} constant onshore wind is included. The duration of a model run is 2 h with a time step of 3 s and an wave-flow

communication interval of 6 s. For output, 300 m of each alongshore end is removed to eliminate potential boundary affected currents.

An individual based model with the transport equations explained in Chapter 2 is applied. All simulations are calculated in Lagrangian framework, so the Stokes drift is always taken into account. Characteristics of released particles are also based on Chapter 2: particles in each case are assigned a vertical velocity either -10^{-3} m s^{-1} or 4×10^{-3} m s^{-1}, and the particles, representing competent larvae, change their vertical velocities to -10^{-2} m s^{-1} where the turbulent energy dissipation rate (ε) is greater than 10^{-5} m^2 s^{-3} (i.e., in the surf zone and at the bottom of wave boundary layer). In this chapter, negatively and positively buoyant particles are always modeled with no-wind and the constant onshore wind, respectively. Two successful larval migration scenarios proposed in Chapter 2 are considered here: negatively buoyant particles migrating toward shore via wave-induced current, especially bottom boundary layer streaming; positively buoyant particles are carried by wind-driven currents, and sink to the bottom once they reach the surf zone edge ($\varepsilon > 10^{-5}$ m^2 s^{-3}) because of the turbulent-dependent sinking behavior, then catch the onshore bottom currents to reach the shore.

The output of 2-h hydrodynamic simulation is used periodically for 48 h. 567 particles equally distributed alongshore ($\Delta Y = 10$ m) are released every hour from offshore, near the bottom for the negatively buoyant particles, and near the water surface positively buoyant particles. Alongshore boundaries of this module are periodic, while the offshore is an outlet boundary (i.e., once particles exit the model domain, they do not return). The first 36-h run is used as a spin-up stage for particle initialization, and only the simulation from 36 h to 48 h is used for analysis.

4.3. Results

Modeling with alongshore uniform beach show that negatively buoyant particles in the no-wind regime enter the surf zone more at milder sloping beaches (Fig. 4.3A,C). Note that the surf zone width gets narrower at a steeper slope beach. A high concentration area of negatively buoyant particles is inside the surf zone at a mild sloping beach, and gradually shifts toward offshore as a beach slope becomes steeper. Those particles are concentrated just outside the surf zone at steep beaches. Most negatively buoyant particles at steep beaches are flushed out of the domain. On the other hand, positively buoyant particles in the onshore wind regime with any beach slope neither enter the surf zone nor exit the domain, but stay just outside the surf zone (Fig. 4.3B). A beach slope is not correlated with a concentration of positively buoyant particles in the surf zone, and very weakly correlated with that in the domain (Fig. 4.3C).

By adding rip-channels and shoals, the number of transported particles inside the surf zone increases both in the negatively buoyant particle case (Fig. 4.4A) to 1.12 times more, and positively buoyant particle case (Fig. 4.4C) to 81.06 times more than the case of the alongshore uniform beach. Both types of particles with the assigned wind regimes are highly concentrated at rip channels, which is consistent with the model cases and field observation at Sand City beach in Chapter 2.

Wave group forcing also helps onshore transport of the positively buoyant particle (Fig. 4.4D). Those particles increase by 51.63 times from the regular wave case. However, the negatively buoyant particles are reduced by 1.12 times in the wave group case (Fig. 4.4B).

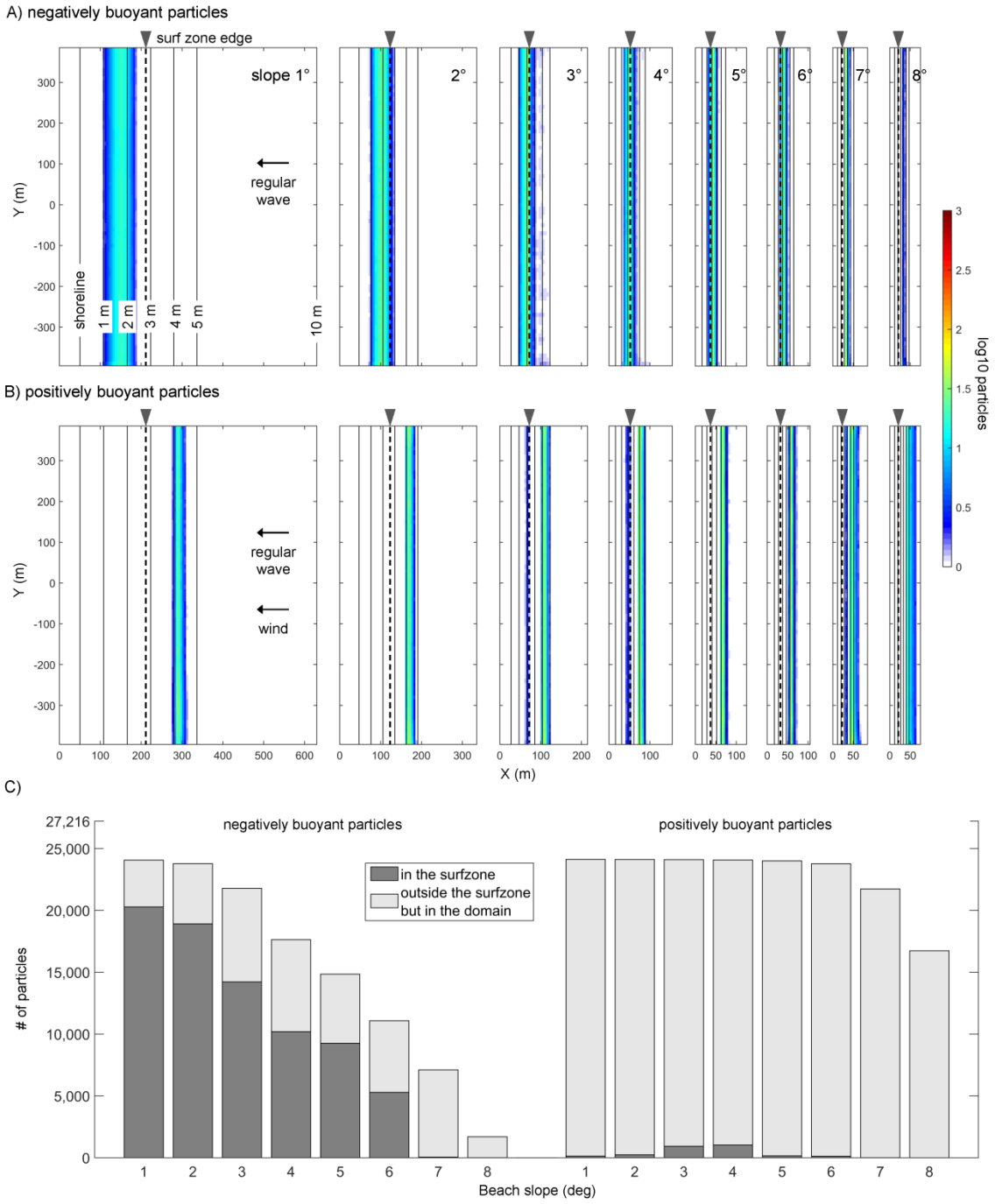

Fig. 4.3. Depth- and time-averaged number of particles per grid cell in (A) negatively buoyant particles in the no-wind cases, and (B) positively buoyant particles in the onshore wind cases. An approximate surf zone edge is indicated by a dashed line and pointed by an arrow head. Contour lines are given from 0 m (shoreline) to 5 m. The right end of each model domain is 10 m. (C) Time-averaged number of particles as a function of beach slope. The upper limit of the vertical axis (27,216) is a total number of particles in each simulation.

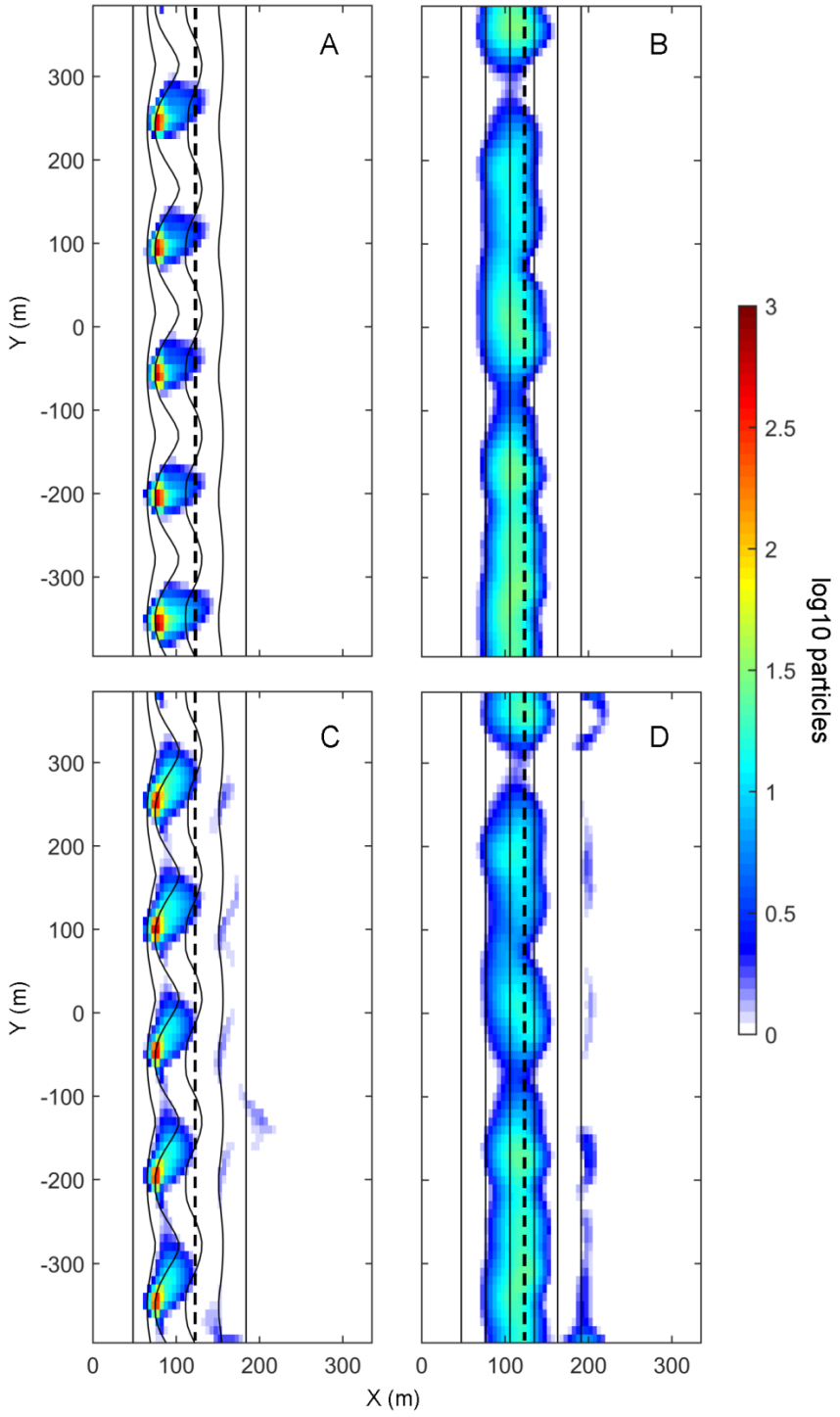

Fig. 4.4. Depth- and time-averaged number of particles per grid cell at a beach with 2° slope. (A, B) negatively buoyant particles in the no-wind regime. (C, D) positively buoyant particles in the onshore wind regime. (A, C) The bathymetry contains rip channels and shoals. (B, D) Wave groups are included. An approximate surf zone edge is indicated by a dashed line. Contour lines are given from 0 m (shoreline) to 5 m.

4.4. Discussion

The model calculations suggest that onshore larval transport rate can be higher at a more dissipative beach than at a more reflective beach, consistent with the field study by Shanks et al. (2010). In the model at alongshore uniform beaches, this is applicable only for negatively buoyant particles. Most positively buoyant particles at an alongshore uniform beach do not enter the surf zone because wind-driven currents are not strong enough to get the particles to the turbulent zone above the threshold for larval sinking behavior ($\varepsilon > 10^{-5}$ m^2 s^{-3}), which is about X < 140 m. Onshore surface currents shift to offshore at about X = 160 m (Fig. 4.5A, D), where the most particles are stuck (2° slope case in Fig. 4.3B). The same thing happens to every onshore wind case with a different slope, and causes the accumulation of positively buoyant particles just outside the surf zone.

Rip channels and shoals help onshore transport of both types of particles. Rip currents transport material out of the surf zone, but at the same time onshore currents over the shoals are enhanced to conserve a mass balance. The onshore currents well cover the area (Fig. 4.5B) where positively buoyant particles are stuck due to switching the wind-driven onshore current to offshore current (Fig. 4.5D). Those particles enter over the shoals and are caught by a rip circulations, making high concentrations in the rip channels as described in Chapter 2.

At this point, it can be said that the onshore larval transport rate by means of the larval concentration in the surf zone is higher at Sand City beach than CRSB because its slope is milder and it has more alongshore variability (i.e., rip channels).

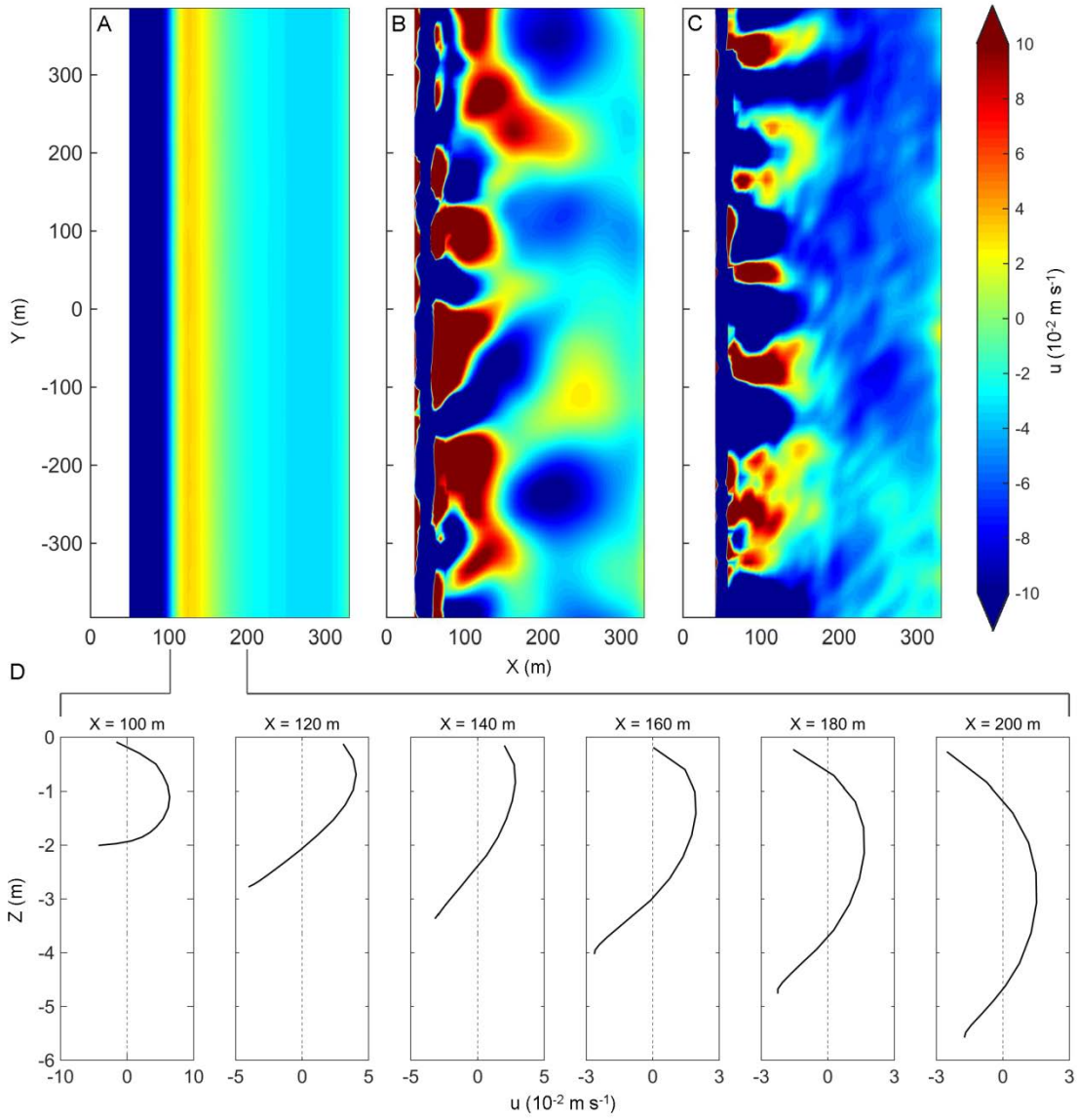

Fig. 4.5. Snapshots (at t = 120 min) of cross-shore surface velocities in the onshore wind, 2° beach slope regime with (A) regular waves at the alongshore uniform beach, (B) regular waves at the rip-channeled beach, and (C) wave groups at the alongshore uniform beach. (D) Vertical profiles of alongshore-averaged cross-shore velocities in the case of (A).

Random wave groups add a similar effect as rip currents to an alongshore uniform beach (Fig. 4.5C). These are transient rip currents which are not topographically controlled and appear randomly (Johnson & Pattiaratchi 2004, Reniers et al. 2004). Similarly to the rip-channeled beach, water mass in the surf zone needs feeder currents to compensate the loss due to transient rip currents. The onshore directed feeder currents carry the particles to the surf zone. Wave group forcing benefits the positively buoyant particles and increases the concentration of the particles in the surf zone. However, wave group is disadvantageous for onshore transport of the negatively buoyant particles because the particles are pushed offshore by transient rip currents more than that are taken in the surf zone by onshore currents.

In this chapter three factors are shown to be variables of onshore larval transport. A steeper (more reflective) beach repels larvae more than a gradual (more dissipative) beach does. Migrating larvae reach the surf zone at a rip-channeled beach better than at a beach with less alongshore variability. Depending on the characteristics of larvae, wave group forcing can enhance onshore larval delivery.

Chapter 5

CONCLUDING REMARKS

5.1. Conclusion

This work provides plausible explanations of onshore transport of competent intertidal invertebrate larvae, and fills the gap in knowledge of larval transport. When the larvae cross the surf zone, which acts as a semi-permeable barrier (Rilov et al. 2008, Shanks et al. 2010), biological, physical, and geological factors are involved in the transport process.

At the rip-channeled beach (Sand City), two possible scenarios are proposed: negatively buoyant larvae without wind forcing sink in the turbulent bottom boundary layer and are carried onshore by streaming; positively buoyant larvae drift toward shore in wind-driven surface currents to the surf zone, then sink in the turbulent surf zone and remain near the bottom while transported shoreward. The larvae in both cases are eventually trapped by rip circulations, resulting in high larval concentrations in rip-channels. These scenarios can be achieved only if turbulence-dependent sinking behavior and Stokes drift are included in the transport of larvae.

The onshore larval delivery rate at the steep pocket beach (CRSB) is less than the rip-channeled beach. Because of the beach configuration and wave angle, an alongshore current and small eddies control the distribution of larvae. The distribution pattern of negatively buoyant larvae is similar to that of detritus. Additionally, the concentrations of detritus and competent larvae within the surf zone are negatively correlated with wave

height, consistent with the observations of the accompanied field study (Shanks et al. 2015).

To understand the difference in onshore larval transport at Sand City beach and CRSB, beach topography is decomposed. Modeling with alongshore uniform beaches show that a gradual sloping beach attract more larvae than a steeper beach, consistent with Shanks et al. (2010). Forming rip-channels and shoals help larval transport toward shore through rip-current-compensated onshore currents over the shoals. Therefore, larvae are found in the surf zone at Sand City beach, a mildly sloping rip-channeled beach, more than the surf zone at CRSB, a less alongshore variable steep slope beach. Wave group forcing adds an effect similar to alongshore variability by producing transient rip currents. These non-topographic oriented rip currents induce feeding onshore currents which take larvae into the surf zone.

5.2. Future Work and Suggestions

Tidal forcing can affect larval transport (Shanks 1986, Pineda 1999), especially timing of onshore migration. Tidal elevation also affects the surf zone hydrodynamics. At Sand City, rip currents are strong at low tide and are weaken at high tide, thus cross-shore exchange should be enhanced during low tide and suppressed during high tide. CRSB becomes less reflective when tidal elevation is low, so larvae or particles probably get into the surf zone relatively easy during low tide. At the northern end of the beach, local counterclockwise circulation may be pronounced during low tide, possibly due to reduced overwash on the north rocks. Some particles may be trapped here. In addition to tides, diurnal wind stresses are important cross-shore transport of water, as found by

Hendrickson and MacMahan (2009). Larvae residing near the bottom are transported shoreward during wind relaxation or offshore wind events, whereas larvae residing near the surface are transported shoreward during onshore wind events. Therefore, long-term simulations are necessary to gauge the effects of tide and wind as well as waves for deep understanding in the effects of wave height, period, and angle on larval transport. A long-term hydrodynamic modeling of CRSB is especially of interest because the beach hydrodynamics are not well known comparing to Sand City beach. For CRSB, as a steep beach, wave reflection would be included to see if it causes to keep particles away from the surf zone.

The model used throughout this study does not include breaking wave roller, which may entrain some particles and carry them to the shore (Feddersen 2007, Reniers et al. 2013), thus it is worth to test its contribution to onshore particle transport.

Species-specific modeling is also essential. Sinking rate and swimming speed of larvae vary among the species (Chia et al. 1984). Larvae of each species also have different depth preference. Vertical migrations of larvae can be ontogenetically, and also related to tidal and diel cycles, again depending on species. Horizontal swimming could also be important for cross-shore migration by relatively strong swimming fish and crab larvae. Horizontal swimming directions might be determined by multiple environmental stimuli (e.g., sound, sunlight, and chemical signals) and studies on these orientation behaviors should improve larval transport in general.

At Sand City beach, holoplankton organisms such as copepods were also more concentrated in the surf zone than offshore although they are pelagic species. Because

turbulent-dependent sinking behavior has not been reported for this group, it is probably necessary to consider the other mechanism for them to reach the shore.

The biophysical model used in this study can be applicable to transport of phytoplankton as well. During the field campaign, phytoplankton samples were also collected. Preliminary results show that phytoplankton cells are mostly concentrated in the surf zone rather than offshore at Sand City, and concentrated offshore at CRSB. The results are somewhat similar to that of zooplankton; however, phytoplankton can only swim very weakly comparing to zooplankton or does not swim at all, and cells are generally almost neutrally buoyant. How can the cross-shore transport of phytoplankton, as passive particles, be possible? Adding phytoplankton-specific parameter(s) to the biophysical model may help to answer.

REFERENCES

Battjes JA (1974) Surf similarity. Coast Eng 1:466–479

Brown JA, MacMahan JH, Reniers AJHM, Thornton EB, Shanks AL, Morgan SG, Gallagher EL (in review) Mixing and Transport on a Steep Beach

Butman CA (1987) Larval settlement of soft-sediment invertebrates: the spatial scales of pattern explained by active habitat selection and the emerging role of hydrodynamical processes. Oceanogr Mar Biol Annu Rev 25:113–165

Butman CA (1989) Sediment trap experiments on the importance of hydrodynamical processes in distributing settling invertebrate larvae in near-bottom waters. J Exp Mar Biol Ecol 134:37–88

Chia F-S, Buckland-Nicks J, Young CM (1984) Locomotion of marine invertebrates: a review. Can J Zool 62:1205–1222

Connolly SR, Menge BA, Roughgarden J (2001) A latitudinal gradient in recruitment of intertidal invertebrates in the northeast Pacific Ocean. Ecology 82: 1799–1813.

Dalrymple RA, MacMahan JH, Reniers AJHM, NelkoV (2011) Rip currents. Ann Rev Fluid Mech 43:551–581, doi:10.1146/annurev-fluid-122109-160733

Deltares (2011a) Delft3D-FLOW User Manual, Version 3.15, Delft,the Netherlands: Deltares. http://oss.deltares.nl/documents/183920/185723/Delft3D-FLOW_User_Manual.pdf

Deltares (2011b) Delft3D-WAVE User Manual, Version 3.04, Delft,the Netherlands: Deltares. http://oss.deltares.nl/documents/183920/185723/Delft3D-WAVE_User_Manual.pdf

Denny MW, Shibata MF (1989) Consequences of surf-zone turbulence for settlement and external fertilization. Am Natur 134:859–889

Feddersen F. (2007) Breaking wave induced cross-shore tracer dispersion in the surfzone: Model results and scalings, J Geophys Res 112:C09012, doi:10.1029/2006JC004006

Fewings M, Lentz SJ, Fredericks J (2008) Observations of cross-shelf flow driven by cross-shelf winds on the inner continental shelf. J Phys Oceanogr 38: 2358–2378, doi:10.1175/2008JPO3990.1

Fuchs HL, Huter EJ, Schmitt EL, Guazzo RA (2013) Active downward propulsion by oyster larvae in turbulence. J Exp Biol 216:1458–1469, doi:10.1242/jeb.079855.

Fuchs HL, Mullineaux LS, and A. R. Solow (2004) Sinking behavior of gastropod larvae (*Ilyanassa obsoleta*) in turbulence. Limnol Oceanogr 49:1937–1948

Hasselmann K, Barnett TP, Bouws E, Carlson H, Cartwright DE, Enke K, Ewing JA, Gienapp H, Hasselmann DE, Kruseman P, Meerburg A, Mueller P, Olbers DJ, Richter K, Sell W, Walden H (1973) Measurements of wind-wave growth and swell decay during the Joint North Sea Wave Project (JONSWAP). Dtsch Hydrogr Z Suppl A(8):12, 95 pp

Hendrickson J, MacMahan J (2009) Diurnal sea breeze effects on inner-shelf cross-shore exchange. Cont Shelf Res 29:2195–2206, doi:10.1016/j.csr.2009.08.011

Johnson D, Pattiaratchi C (2004) Transient rip currents and nearshore circulation on a swell-dominated beach. J Geophys Res 109:C02026, doi:10.1029/2003JC001798

Kingsford MJ, Leis JM, Shanks A, Lindeman KC, Morgan SG, Pineda J (2002) Sensory environments, larval abilities and local self-recruitment. Bull Mar Sci 70:309–340

Lentz, SJ, Fewings, M, Howd, P, Fredericks, J, Hathaway, K (2008) Observations and a model of undertow over the inner continental shelf. J Phys Oceanogr 38: 2341–2357, doi:10.1175/2008JPO3986.1

Longuet-Higgins MS (1953) Mass transport in water waves. Philos Trans Roy Soc London, A245:535–581

MacMahan JH, Brown J, Brown J, Thornton E, Reniers A, Stanton T, Henriquez M, Gallagher E, Morrison J, Austin MJ, Scott T, Senechal N (2010) Mean Lagrangian flow behavior on an open rip-channeled beach: a new perspective. Mar Geol 268:1–15, doi:10.1016/j.margeo.2009.09.011

MacMahan J, Reniers AJHM, Thornton EB, Stanton TP (2004) Infragravity rip current pulsations. J Geophys Res 109:C01033, doi:10.1029/2003JC002068

Mileikovsky SA (1973) Speed of active movement of pelagic larvae of marine bottom invertebrates and their ability to regulate their vertical position. Mar Biol 23:11–17

Morgan SG, Fisher JL (2010) Larval behavior regulates nearshore retention and offshore migration in an upwelling shadow and along the open coast. Mar Ecol Prog Ser 404:109-126, doi:10.3354/meps08476

Morgan SG, Fisher JL, Mace AJ (2009a) Larval recruitment in a region of strong, persistent upwelling and recruitment limitation. Mar Ecol Prog Ser 394:79–99, doi:10.3354/meps08216

Morgan SG, Fisher JL, Mace AJ, Akins L, Slaughter AM, Bollens SM (2009b) Cross-shelf distributions and recruitment of crab postlarvae in a region of strong upwelling. Mar Ecol Prog Ser 380: 173–185, doi:10.3354/meps07913

Morgan SG, Fisher JL, Miller SH, McAfee ST, Largier JL (2009c) Nearshore larval retention in a region of strong upwelling and recruitment limitation. Ecology 90:3489–3502, doi:10.1890/08-1550.1

North EW, Gallego A, Petitgas P (2009) Manual of recommended practices for modelling physical-biological interactions during fish early life. ICES Coop Res Rep 295, ICES

Paris CB, Atema J, Irisson J-O, Kingsford M, Gerlach G, Guigand CM (2013*a*) Reef odor: A wake up call for navigation in reef fish larvae. PLoS ONE 8:e72808, doi:10.1371/journal.pone.0072808

Paris CB, Chérubin L, Cowen R (2007) Surfing, spinning, or diving from reef to reef: effects on population connectivity. Mar Ecol Prog Ser 347: 285–300, doi:10.3354/meps06985

Paris CB, Helgers J, Van Sebille E, Srinivasan A (2013) Connectivity Modeling System: A probabilistic modeling tool for the multi-scale tracking of biotic and abiotic variability in the ocean. Environ Modell Softw 42: 47–54, doi:10.1016/j.envsoft.2012.12.006

Pineda J (1999) Circulation and larval distribution in internal tidal bore warm fronts. Limnol Oceanogr 44:1400–1414

Queiroga H, Blanton J (2005) Interactions between behaviour and physical forcing in the control of horizontal transport of decapod Crustacean larvae. Adv Mar Biol 47:107–214, doi:10.1016/S0065-2881(04)47002-3

Reniers AJHM, Gallagher EL, MacMahan JH, Brown JA, van Rooijen AA, van Thiel de Vries JSM, van Prooijen BC (2013) Observations and modeling of steep-beach grain-size variability. J Geophys Res 118:577–591, doi:10.1029/2012JC008073

Reniers AJHM, MacMahan JH, Beron-Vera FJ, Olascoaga MJ (2010) Rip-current pulses tied to Lagrangian coherent structures. Geophys Res Lett 37:L05605, doi:10.1029/2009GL041443

Reniers AJHM, MacMahan JH, Thornton EB, Stanton TP, Henriquez M, Brown JW, Brown JA, Gallagher E (2009) Surf zone retention on a rip-channeled beach. J Geophys Res 114:C10010, doi:10.1029/2008JC005153

Reniers AJHM, Roelvink JA, Thornton EB (2004) Morphodynamic modeling of an embayed beach under wave group forcing. J Geophys Res 109:C01030, doi:10.1029/2002JC001586

Rilov G, Dudas SE, Menge BA, Grantham BA, Lubchenco J, Schiel DR (2008) The surf zone: A semi-permeable barrier to onshore recruitment of invertebrate larvae? J Exp Mar Biol Ecol 361:59–74, doi:10.1016/j.jembe.2008.04.008

Roughgarden J, Gaines S, Possingham, H (1988) Recruitment dynamics in complex life cycles. Science 241:1460–1466

Roy A, Metaxas A, Ross T (2012) Swimming patterns of larval *Strongylocentrotus droebachiensis* in turbulence in the laboratory. Mar Ecol Prog Ser 453:117–127, doi:10.3354/meps09662

Shanks AL (1995) Oriented swimming by megalopae of several eastern North Pacific crab species and its potential role in their onshore migration. J Exp Mar Biol Ecol 186:1-16

Shanks AL (1986) Tidal periodicity in the daily settlement of intertidal barnacle larvae and an hypothesized mechanism for the cross-shelf transport of cyprids. Biol Bull 170:429-440

Shanks AL, MacMahan J, Morgan SG, Reniers AJHM, Marley J, Brown J., Fujimura A, Griesemer C (2015) Transport of larvae and detritus across the surf zone of a steep reflective pocket beach. Mar Ecol Prog Ser 528:71–86, doi:10.3354/meps11223

Shanks AL, Morgan SG, MacMahan J, Reniers AJHM (2010) Surfzone hydrodynamics as determinants of temporal and spatial variation in larval recruitment. J Exp Mar Biol Ecol 392:140–150, doi:10.1016/j.jembe.2010.04.018

Shanks AL, Shearman RK (2009) Paradigm lost? Cross-shelf distributions of intertidal invertebrate larvae are unaffected by upwelling or downwelling. Mar Ecol Prog Ser 385:189–204, doi:10.3354/meps08043

Staaterman E, Paris CB, Helgers J (2012) Orientation behavior in fish larvae: A missing piece to Hjort's critical period hypothesis. J Theor Biol 304:188–196, doi:10.1016/j.jtbi.2012.03.016

Stokes GG (1847) On the theory of oscillatory waves. Trans Cambridge Philos Soc 8:441–455

Talbot M, Bate G (1987) Rip current characteristics and their role in the exchange of water and surf diatoms between the surf zone and nearshore. Estuar Coast Shelf Sci 25:707–20

Tilburg CE (2003) Across-shelf transport on a continental shelf: Do across-shelf winds matter? J Phys Oceanogr 33:2675–2688

Vermeij MJA, Marhaver KL, Huijbers CM, Nagelkerken I, Simpson SD (2010) Coral larvae move toward reef sounds. PLoS ONE 5:e10660, doi:10.1371/journal.pone.0010660

Wright LD, Short AD (1984) Morphodynamic variability of surf zones and beaches. Mar Geol 56:93–118